UNIVERSITY OF GENEVA

Multi-jet trigger performance and improvements using tracking capability at ATLAS

Author:
Yannick DEMETS

Supervisors:
PROF. ANNA SFYRLA,
DR. TENG JIAN KHOO,
M.SC. MARCO VALENTE

A thesis submitted in fulfillment of the requirements for the degree of Master in physics

in the

Department of Nuclear and Particle Physics

UNIVERSITÉ DE GENÈVE

FACULTÉ DES SCIENCES
Section de physique

June 27, 2019

UNIVERSITY OF GENEVA

Abstract

Science Faculty
Department of Nuclear and Particle Physics

Multi-jet trigger performance and improvements using tracking capability at ATLAS

by Yannick DEMETS

In this thesis performance studies and multi-jet trigger improvements are presented. Rate reductions and efficiencies are evaluated by applying tracking information to the event selections at the trigger level, to reduce the impact of the pile-up. Both topological clustering reconstructed jets and particle flow reconstructed jets are used. The impact of JVT selections in the rate gives a reduction of 30% to 40%. For different JVT values there is no significant impact on the rate reduction as on the efficiency. The efficiency curves improve when using a JVT cut at trigger level. Further, performance studies of Run2 data are done and close-by inefficiencies are examined.

Acknowledgements

I would like to thank Prof. Anna Sfyrla for giving me the opportunity to complete this project and always be present for helping me whenever I had any questions about my project or writing. Also, I would like to thank Dr. Teng Jian Khoo for guiding me and providing me with answers and help whenever needed. I would also like to thank Macro for helping me and the support along the way. To all the group a big thank you for the experience in a positive atmosphere.

Contents

List of Figures

Chapter 1

Introduction

The LHC is currently the most powerful particle accelerator in the world producing proton-proton collisions at centre of mass energies of around 13 TeV. ATLAS is one of the four majors experiments, where proton bunches are made to collide and produce many particles to be detected. These collisions provide many scatterings of which some are relevant for physics and some are not. Those other interactions which are soft scattering processes are also known as *pile-up* interactions and do not produce new interesting physics phenomena and can influence the interesting hard scattering processes. For this, different methods are used to suppress the influence of the soft scattering processes.

The trigger at ATLAS is an important system of the experiment. It is the data acquisition and the trigger system which are responsible for the selection and the recording of the data with the physics of interest. The trigger must take a fast decision, what limits the capability for complicated event reconstruction, including full-detector tracking in the CPU farm. A workaround to this problem is given by FTK, a new hardware component that will provide the trigger with good tracks of similar quality to offline. This will help when applying offline-like selections at trigger level, such as sophisticated track-based pile-up suppression techniques.

In this study a track-based pile-up suppression at the trigger level is investigated looking at the rate reductions and the efficiencies of some specific trigger chains. The thesis is organised as follows. The LHC and the ATLAS detector are described in Chapter 2. Follows in Chapter 3, the explanation of jets along with the reconstruction algorithm used. In Chapter 4, the ATLAS trigger system is explained and described. The performance studies and the results are presented in Chapter 5, following with a conclusion in Chapter 6.

Chapter 2

The Experiment

The European Organisation for Nuclear Research (CERN) is an international organisation founded in 1954 and is one of the most important institutions for high energy physics in the world. It is located close to Geneva at the border between Switzerland and France. CERN operates the Large Hadron Collider (LHC).

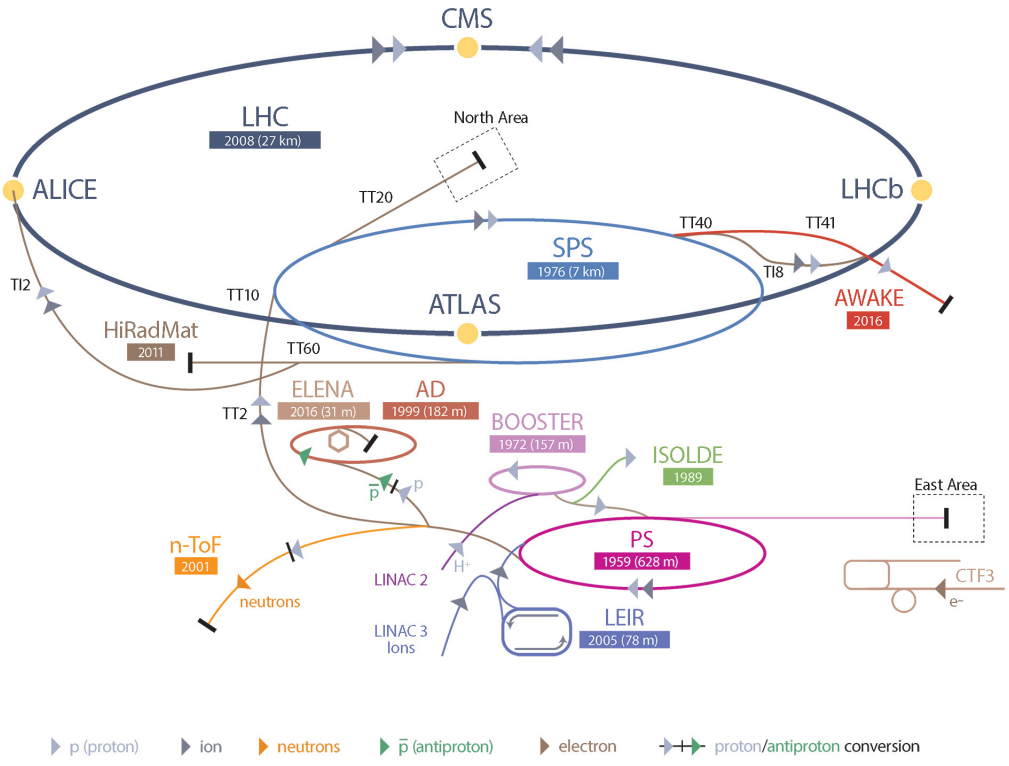

FIGURE 2.1: CERN Accelerator Complex. ©CERN

2.1 The Large Hadron Collider

The LHC is at the moment, the world's largest and the most powerful proton-proton collider. The main ring of the LHC is built in a tunnel with circumference of 26.7 km and at depth varying between 45 and 170 m. The accelerator uses the tunnel from the previous experiment : the Large Electron-Positron (LEP). In 2010, the LHC started to operate at a centre-of-mass energy of $\sqrt{s} = 7$ TeV which was increased to $\sqrt{s} = 8$ TeV

in 2012. After a first long shutdown for two years (LS1) , it started again operating in 2015 with nearly twice the centre-of-mass energy $\sqrt{s} = 13\,\text{TeV}$.

To accelerate protons to these energy ranges different accelerators and components are necessary (figure 2.1). Before injecting the particles into the LHC there must be a pre-acceleration happening. The protons are coming from ionised hydrogen atoms. Then arriving in the linear accelerator LINAC2 where the proton beam is injected into the BOOSTER. At that point the proton beam reaches an energy of 1.4 GeV. The beam is then sent to the Proton Synchrotron (PS), achieving an energy of 25 GeV. After this, they arrive at the Super Proton Synchrotron (SPS) where the protons are accelerated to an energy of 450 GeV. They are then transferred into the LHC and split in clockwise and anti-clockwise beams. Each proton beam consists of 2808 bunches where each bunch has about 600 million protons. The beam follows a circular trajectory which is done using magnetic fields of about 8T.

There are four main experiments located at four distinct points following the beam's path at the LHC. Those are four interaction points where the beams can collide. The four main experiments are :

- A Toroidal LHC ApparatuS (ATLAS) (Section 2.2) and a Compact Muon Solenoid (CMS) that are both general purpose experiments sharing the same physics goals. ATLAS is the biggest one and it is located at the opposite side of CMS. CMS is a more compact experiment where tracker and calorimeter are wrapped within a single large solenoid magnet. Those two experiments are complementary.

- A Large Ion Collider Experiment (ALICE) which is an experiment designed to study heavy ion collisions. This is done to have a better understanding of the physics with the conditions of the early universe. Meaning by this, studying strongly interacting matter and a quark-gluon plasma which is a state of matter at high temperature and density.

- LHC beauty (LHCb) which is an experiment that aims to help explain the matter-antimatter asymmetry of the Universe. It studies primarly the parameters of the CP violation in the interactions and rare decays of b hadrons.

Also other experiments are using the beam line of the LHC such as TOTEM [14] , LHCf [10] or the MoEDAL [41].

The initial design centre-of-mass energy of the LHC is 14 TeV. One important phenomenon is the energy loss by synchrotron radiation. The accelerating protons in the LHC emit electromagnetic radiation, which we call synchrotron radiation, and lose energy. The energy loss by synchrotron radiation is proportional to $1/m^4$, where m is the mass of the moving particle in the ring. It can be understood that the energy loss by electromagnetic radiation of protons is lower than for electrons because electrons are lighter than protons. So one of the advantages of proton-proton colliders compared with electron-positron colliders is for example that it can achieve a higher centre-of-mass energy because of the lower energy loss of protons.

An important parameter in particle physics experiments is the luminosity L, which is the quantity that measures the ability of a particle accelerator to produce the required number of interactions. In other words, the luminosity is a measure of how efficiently a particle accelerator produces collision events. This needs to be

high enough to have the most events possible and so have the physics of interest. It is the proportionality factor between the number of events per second $\frac{dN}{dt}$ and the cross section σ_p:

$$\frac{dN}{dt} = L \times \sigma_p \tag{2.1}$$

Because the dimension of the cross section is a surface, the units of luminosity are $cm^{-2}s^{-1}$. The luminosity for head-on colliding beams as the LHC is defined as followed:

$$L = \frac{N_1 N_2 f N_b}{4\pi\sigma_x\sigma_y} \tag{2.2}$$

with N_1 and N_2 the number of particles per bunch for each colliding beam, f the revolution frequency and N_b the number of bunches. The parameters σ_x and σ_y characterise the transverse beam sizes in the horizontal and vertical directions. The assumption that the bunches are identical in transverse profile, that the profiles are Gaussian and independent of position along the bunch is performed for the equation (2.2).

The beam size is described by two quantities: the transverse emittance ϵ and the amplitude function (beta function) β. First, the transverse emittance is a parameter which translates the quality of the beam. Emittance can be described as the area of the beam in phase space. For example a low emittance particle beam is a beam where the particles are close to each other and confined to a small distance to each other and therefore have nearly the same momentum. The second quantity, the amplitude function which is set by the magnet configuration and more precisely by the focussing of the quadrupole magnets. The width of the beam is the product of emittance and the amplitude function. So to achieve a narrow beam the emittance and the amplitude function need to be small. So in the purpose of having a higher probability of increasing the number of collisions the β needs to be as low as possible. More important it is at the interaction point of the opposing beams that the beta (β^*) needs to be as low as possible and those quantities the luminosity can be rewritten as follow :

$$L = \frac{N_1 N_2 f N_b}{4\epsilon\beta^*} \tag{2.3}$$

So to achieve higher luminosity, what is needed is to have the number of particles per bunch N_1, N_2 high. With a low emittance ϵ to collide high at frequency and where at the interaction point the β^* is as low as possible. [36]

From Run1 to Run2 of the LHC the peak luminosity has increased by a factor of three. Keeping the bunch collision rate constant, this can be done in two ways : [31]

1. By increasing the number of protons per bunch. This will then increase the probability that protons from opposing bunches will collide when crossed.

2. By reducing the cross-sectional area of overlap between the beams. This means more precisely decreasing the transverse beam size at the interaction point. This is done by reducing the beta function at that particular point, which is also called "squeeze".

This way the luminosity increases but keeps the bunch rate constant. The spacing between the bunches or in other words the timing between the bunches is of 25 ns for the Run 2. The squeeze does not affect the longitudinal bunch separation. Longitudinal properties of the beam are controlled via the Radio Frequency system

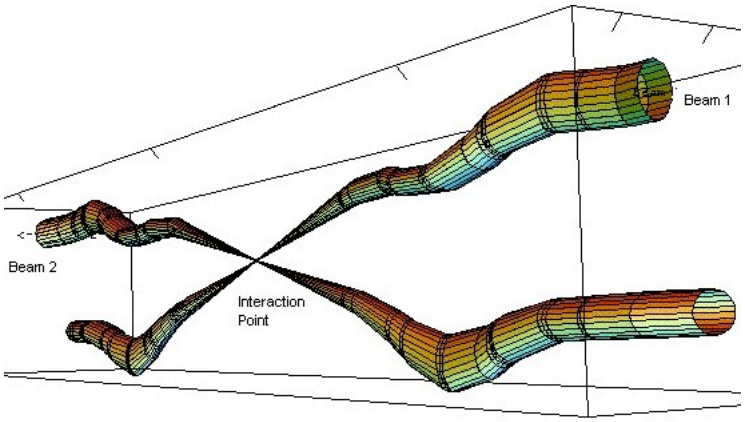

FIGURE 2.2: Beta function, relative beam sizes around IP1 (Atlas) in collision. [20]

(RF). Transverse properties of the beam are controlled, in the absence of emittance growth or shrink, by the magnets of the accelerator lattice. So only the RF system can change the longitudinal beam size. [31]

2.2 ATLAS

The ATLAS detector is one of the four major experiments at CERN. It is located at one of the interaction points of the LHC ring. The detector (figure 2.3) has a cylindrical symmetry with respect to the beam axis. It has a length of 44 m and a width of 25 m. The detector consists of four major sub-detectors. Starting from the interaction point, these are the inner detector (ID), the electromagnetic and hadronic calorimeters and the muon chambers. It is those sub-detectors and the combined information from them that is used to identify the different particles and to measure their kinematics.[3]

2.2.1 ATLAS Coordinate System

ATLAS uses a specific coordinate system. The spatial right-handed Cartesian coordinate system of ATLAS takes as origin the interaction point at the centre of the detector (figure 2.4). The z-axis is defined along the anticlockwise beam axis and the positive x-axes and y-axes point respectively towards the LHC ring centre and vertically upward. The azimuthal angle ϕ is the angle around the z-axis and the polar angle θ is measured with respect to the beam axis.

The polar angle θ is not used that often but instead the rapidity is used:

$$y = \frac{1}{2} ln\left(\frac{E + p_z}{E - p_z}\right) \tag{2.4}$$

with E and p_z the energy and the longitudinal momentum of the particle. When dealing with high relativistic particles it can be assumed that a particle is massless and the equation 2.4 can be approximated with the pseudorapidity :

$$\eta = -ln(tan(\theta/2)) \tag{2.5}$$

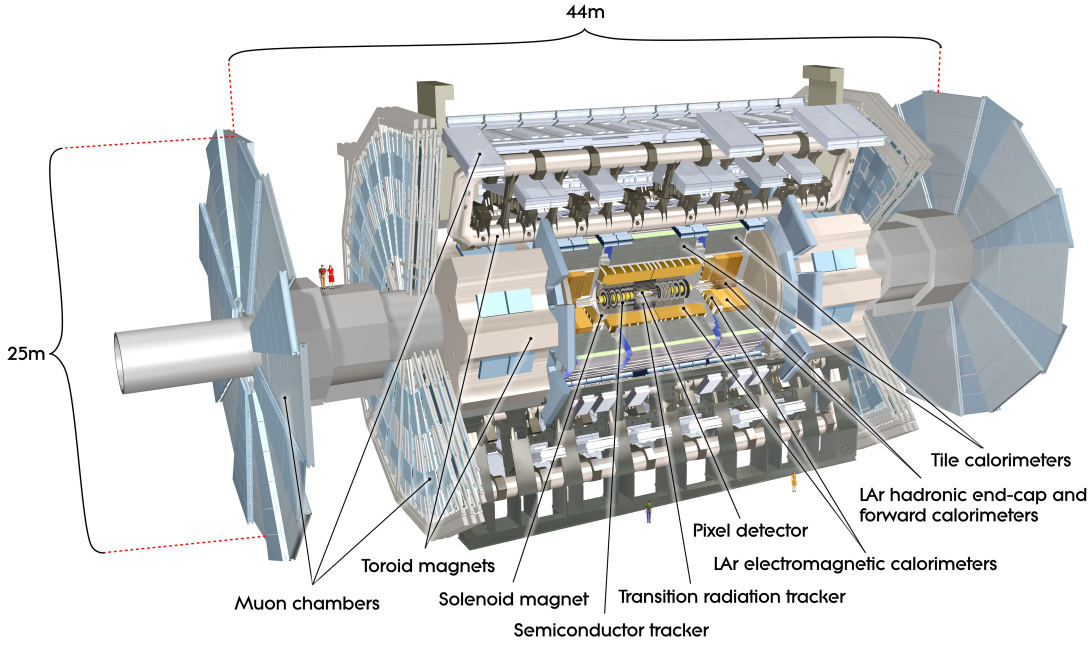

FIGURE 2.3: An overview of the ATLAS detector. ©CERN

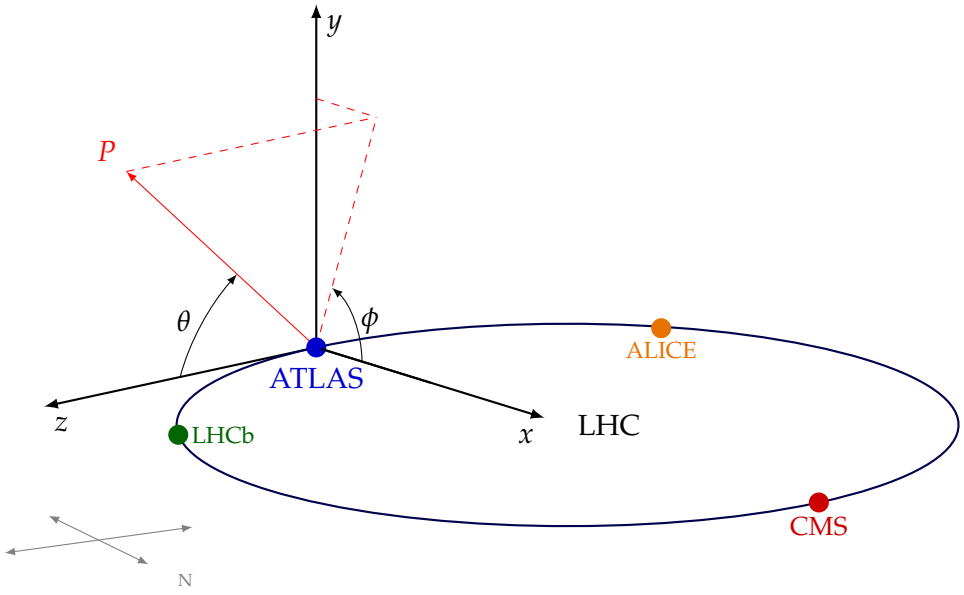

FIGURE 2.4: An overview of 3D ATLAS Coordinate System.

The advantage of using the pseudorapidity is that the differences in η are Lorentz invariant under boost along the beam axis and so particle production is approximately constant in units of pseudorapidity.

Also the angular separation of two objects is given by distances in the $\eta - \phi$ plane ΔR and is defined as :

$$\Delta R = \sqrt{\Delta\eta^2 + \Delta\phi^2} \tag{2.6}$$

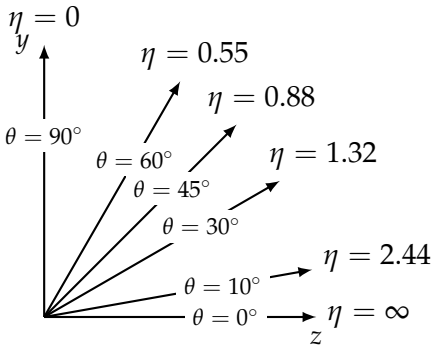

FIGURE 2.5: Pseudorapidity for different polar angles.

The longitudinal momenta of incoming particles are not known in hadron colliders and so the longitudinal momentum conservation is not used. Also too much of the momenta disappears down the beam pipe. But because the incoming particles collide head-on and have no transverse momentum before scattering, the final state particles must have zero total transverse momentum. Therefore the use of the transverse momentum p_T is important. The transverse momentum and the missing transverse momentum E_T^{miss} are both measured in the transverse plane ($x - y$ plane).

2.2.2 Magnets

Before looking at each part of the detector, ATLAS could not well operate if it would be without the magnets. The magnets are used to bend the trajectories of charged particles so that their momenta can be measured. The inner detector is surrounded by a superconducting solenoid magnet that produces a 2 T magnetic field. It is made to be as as thin as possible in order to reduce the energy losses before the particles reach the calorimeters.

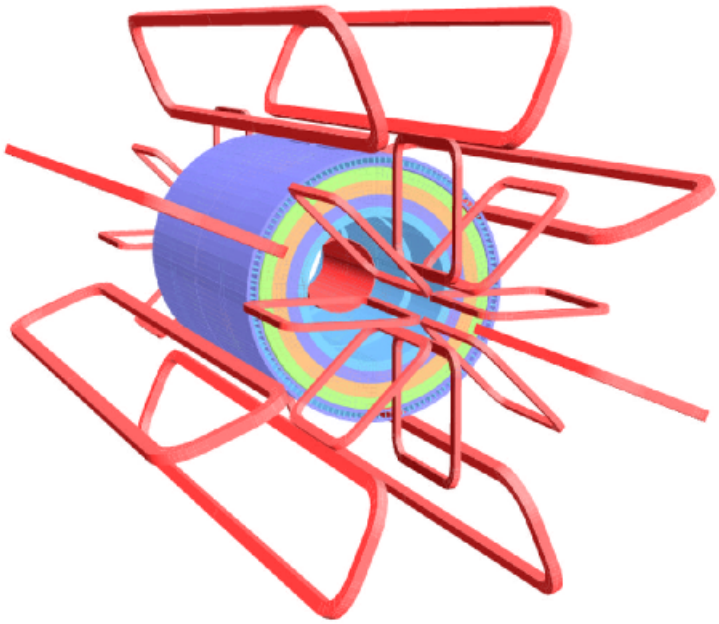

FIGURE 2.6: Schematic view of the ATLAS solenoidal and toroidal magnets. [35]

Large air-core toroids are used to generate a strong magnetic field for the muon chambers located around and inside the structure. This magnet is distinctive to ATLAS because of his toroidal shape. It consists of three parts: one barrel and two endcaps. The barrel surrounds the calorimeters and in the muon spectrometer it consists of a toroid shape. It has height individual empty shapes (figure 2.6). The two endcapes creates a magnetic field for the endcap of the muon spectrometer.

2.2.3 Inner Detector

The first subdetector starting from the beam axis is the Inner Detector, it is the innermost detector of ATLAS. This detector is a tracking detector and its purpose is to reconstruct the tracks of charged particles from the position and momentum information. It covers all the transverse plane. The resolution needs to be high enough to provide precise momentum of the particles as well as distinguishing the vertices from each other.

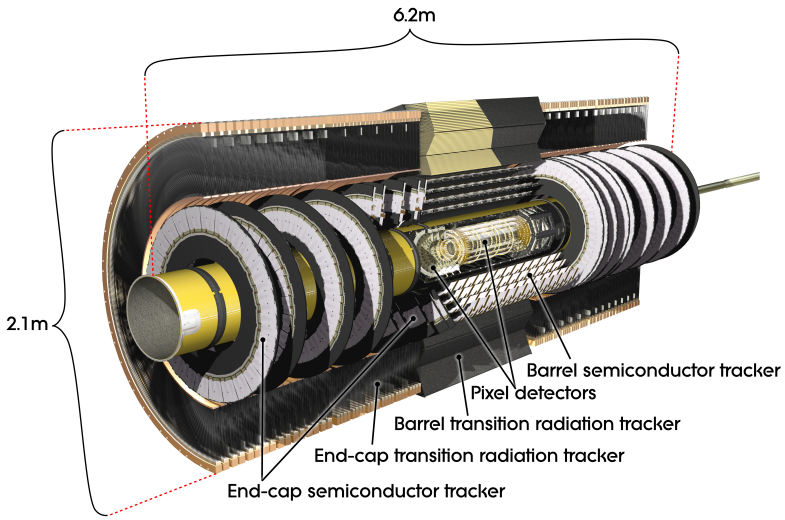

FIGURE 2.7: Schematic view of ATLAS Inner Detector ©CERN

There are four main part inside the Inner Detector (figures 2.7 and 2.8) : the Insertable B-Layer (IBL), the Pixel detector, Semi-Conductor Tracker (SCT) and the Transition Radiation Tracker (TRT). Each of the parts working together to reconstruct the best way possible the tracks of the charged particles. And an import note for latter: it is the data from the IBL, the Pixel detector and the SCT that are used as input for the FTK.

Insertable B-Layer

First starting from the most inner part, the Insertable B-Layer (IBL) who is installed in 2015 as an upgrade. Is consist of an additional layer of the Pixel detector covering $|\eta| < 2.9$ and it improves the tracking performances thanks to smaller pixel occupancy and higher granularity. Due to its position very close to the beam axis, it is especially improving b-tagging and vertex reconstruction. This layer can be replaced easily to keep tracking performance high.[40]

Pixel detector

Surrounding the IBL, there is the actual Pixel detector. This detector consists of pixel modules placed in three cylindrical layers from the beam line. In total having 1744 modules each module made of semi-conducting silicon sensors. The goal of this detector is to give precise the space points of the tracks at each layer and since the pixels are small, the measurement of those space points can be performed with high resolution in two dimensions.[2]

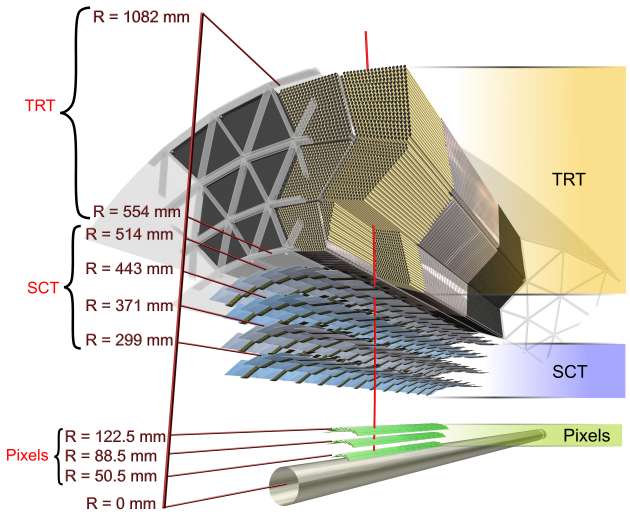

FIGURE 2.8: A cutaway view of ATLAS Inner Detector ©CERN

Semi-Conductor Tracker

Above the pixel detector is placed the Semi-Conductor Tracker (SCT). This tracker has 4088 modules with silicon-strip detectors and consisting of four co-axial cylindrical layers in the barrel ($|\eta| < 1.1$) and two endcaps of 9 disks each ($|\eta| < 2.5$), as shown in Figure 2.9. The silicon-strip detectors have a high granularity and therefore provide precise measurements of momentum and vertex.

The silicon-strip detectors are semiconductor devices made with silicon which is a cheap material and commonly used for such devices. Semiconductors are similar to insulators but have much smaller band-gap which is the difference of energy between the valence band and the conduction band. There are two types of semiconductor : intrinsic and extrinsic. The extrinsic semiconductor can be either n-type material or p-type material. For a n-type a donor donates electrons in the conduction band and for a p-type an acceptor accepts an electron to create a a covalent bond where a hole in the semiconductor's valence band is created. In the case of silicon, it is doped with Arsenic (As) to get a n-type silicon semiconductor or with Boron (B) to get a p-type silicon semiconductor. The junction between p-type and n-type materials is non-conducting when there is no external field applied to it.

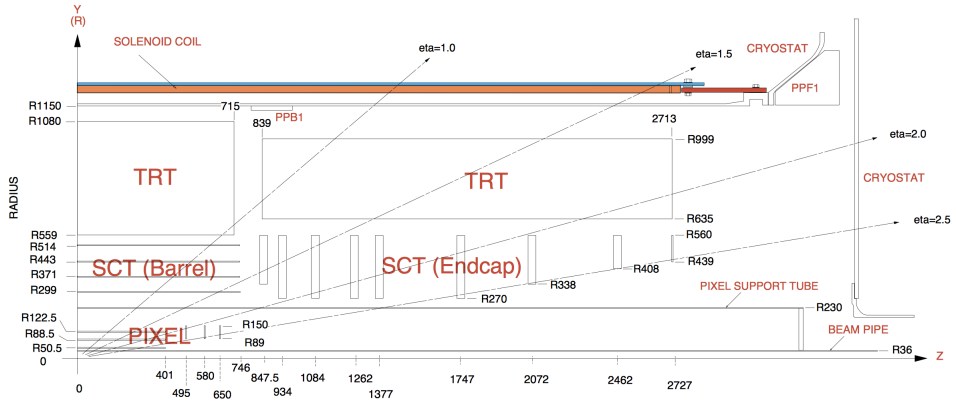

FIGURE 2.9: A schematic view of one quadrant of inner detector with the SCT [8]

At the junction of a p-type and n-type materials, holes leaves the p-side and electrons leaves the n-side. They form negative charged area near the p-side and a positive charged area near the n-side and so creating an electric field. Because of this field, other charge carriers are guided towards the opposite direction. At equilibrium, the result of the electric field effect is a difference in the charge carriers concentration and therefore a diffusion of the carriers counter the drift due to the electric field. This generates a charged area at the junction called depletion region but outside the depletion region, the material is neutral. [39]

The phenomena described in the previous paragraph is used at the detector. When a charged particle penetrates the detector it produces electron-hole pairs along its track. Because of the electric field, the holes drift towards the p-side and the aluminium strips and an electric current is induces such that the spacial information of the interaction can be guessed from the charge associated with each strip.

Transition Radiation Tracker

The last part of the ID, surrounding the SCT is the Transition Radiation Tracker. This is a gaseous detector and is composed of about 300k straws filled with gas mixture and a gold-plated tungsten wire inside. When a charged particle enters this detector it ionises the gas inside the straws. The charges are then collected by applying a electric field between the wire and the boundary of the straw. With this, tracking can be done knowing the points where the charged particle has passed.

2.2.4 Calorimeters

The Calorimeters of ATLAS (figure 2.10) are essential detectors to perform object reconstructions : their purpose is to absorb the energy of particle showers produced by electrons, photons and hadrons emerging from the interaction point. There are two type of calorimeters : electromagnetic calorimeters and hadronic calorimeters. Electromagnetic calorimeters are used to measure the energy of electrons and photons via their electromagnetic interactions with the materials via bremsstrahlung and pair production. Hadronic calorimeters are used to measure the energy of hadrons via

both strong and electromagnetic interactions. In the case of ATLAS, the electromagnetic calorimeter and the hadronic calorimeter are made of a succession of layers of active and absorbing materials, called sampling calorimeters. In works in the following way: when a particle enters the absorbing region an interaction occurs producing secondary particles. These secondary particles produce then again other particles when going deeper into the calorimeter. This produces a cascade of particles called shower and stops when the resulting particles do not have sufficient amount of energy to continue the process. At the same time when the shower proceeds, the particles pass through the active medium which is located between the absorbing layers. This active medium is made of liquid argon and it measures the energy deposits of the particles by detecting the ionisation of the charged particles in the liquid argon. Showers propagate differently depending if they are hadronic or electromagnetic. Electromagnetic showers are induced by electrons or photons and hadronic showers are induced by hadrons. Since the two type of showers are present also two calorimeters are present in ATLAS. Hadronic showers are more complex because part of the energy is carried away by neutrinos which do not interact with the calorimeters, contrary to electromagnetic showers where most of the energy is carried by electrons or photons. [11]

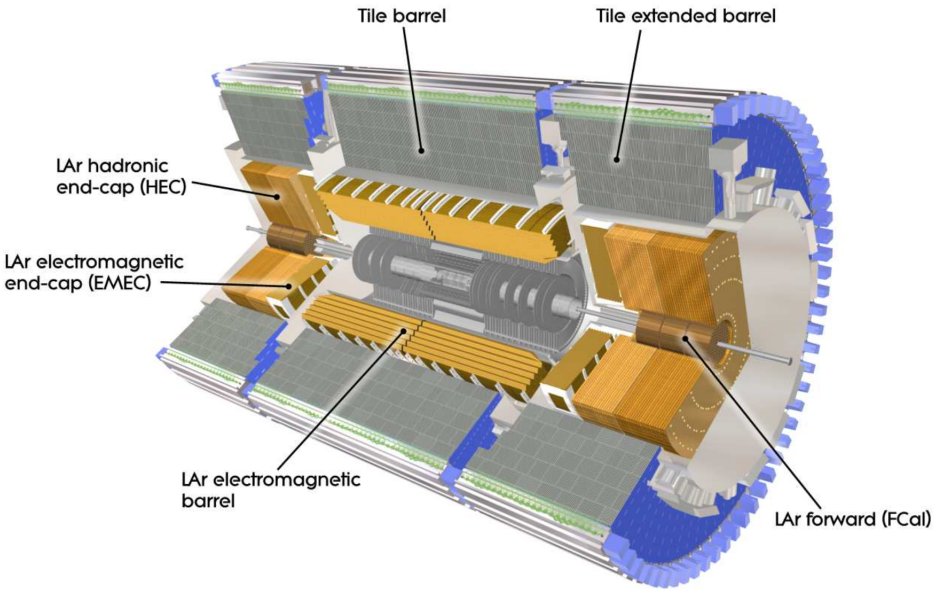

FIGURE 2.10: A view of the ATLAS Calorimeters.[7]

Electromagnetic Calorimeter

The Electromagnetic Calorimeter of ATLAS (ECAL) is a sampling calorimeter. Layers of lead plates of 1.5 mm in thickness with accordion shape and 2.1 mm gap filled with liquid argon are interspaced to form the absorbing material and the active material, respectively. The lead, with its short radiation length, gives the shower development and the secondary electrons create ionisation in the narrow gaps of liquid argon. The ionisation charge is collected then by copper which is also accordion shape. The accordion shape (Figure 2.11) is adopted to cover entire ϕ region without dealing with crack regions which are regions that are not (or only partially) sensitive

to particles developing showers. It also enables to do fast signal extraction at the rear and the front of the electrodes.

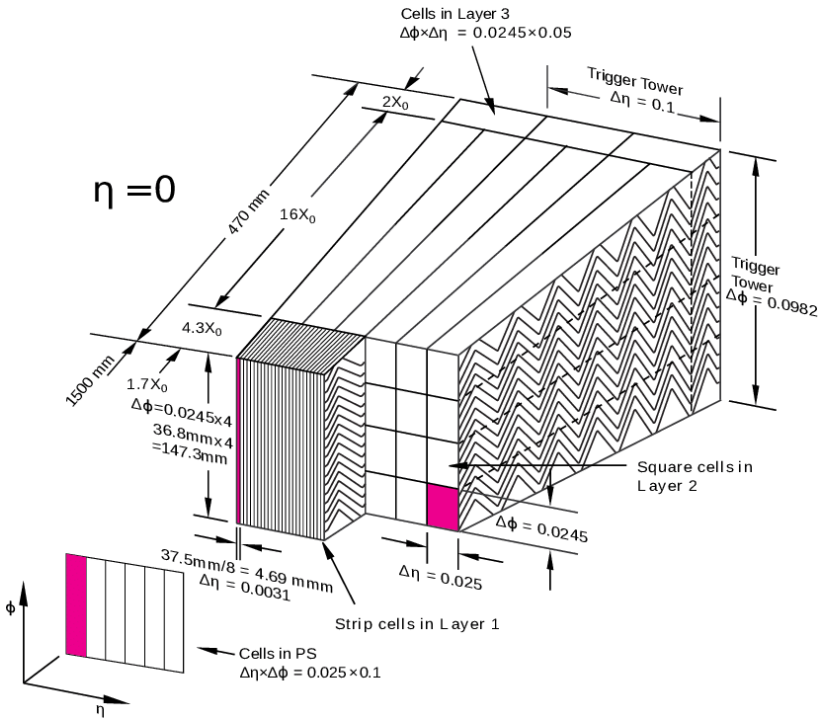

FIGURE 2.11: Schematic view of the ECAL accordion structure.[24]

The ECAL is divided into a barrel part for $|\eta| < 1.475$ and two endcap components for $1.375 < |\eta| < 3.2$. The barrel part has a thickness of at least 22 X_0 where X_0 is the radiation length representing the path length travelled by an electromagnetic interacting particle in a material before loosing $1/e$ of its original energy. The endcap has a thickness that varies as a function of η between $24X_0$ and $38X_0$.[18]

Hadronic Calorimeter

Surrounding the EM calorimeter there is the Hadronic Calorimeter (HCAL) which consists of one tile calorimeter ($|\eta| < 1.7$) and two Hadronic Endcap Calorimeters ($1.5 < |\eta| < 3.2$). There is also a forward region ($3.1 < |\eta| < 4.9$) where a liquid argon calorimeter provides both electromagnetic and hadronic energy measurements. It uses liquid argon as active material but uses different absorbing materials for each layer. The tile calorimeter uses steel plates as absorbing material and plastic scintillators as active material. The tile calorimeter has a central barrel covering up to $|\eta| < 1$ and two extended barrels providing a coverage of $0.8 < |\eta| < 1.7$. The Hadronic Endcap Calorimeter consists of two wheels placed behind the Electromagnetic Calorimeter. It uses cooper plates as absorbing material and liquid argon cooled dow as active material and covers $1.5 < |\eta| < 3.2$. [19] [13]

2.2.5 Muon Spectrometer

The muon spectrometer is the outermost detector of ATLAS, covering the inner detector and the calorimeters. The goal of the muon spectrometer is to track and measure the momentum of the muons which passes the calorimeters with minimal energy loss. The muons are deviated in the magnetic field provided by the large superconducting air-core toroid magnets. The tracks are reconstructed using high-precision tracking chambers for a good muon momentum resolution. The tracking chambers consist of monitored drift tube and of cathode strip chambers for larger $|\eta|$ in between $2 < |\eta| < 2.7$.

2.2.6 Identification

ATLAS uses all those sub-detectors for gathering the necessary information to reconstruct all the different objects, and associate them to particles. The identification is done in steps depending on which objects enter the ATLAS detector. The different objects identified are explained in the following paragraphs.

The protons interact strongly and therefore leave a shower in the HCAL. Also because they are charged they leave tracks in the inner detector and in the ECAL. On the contrary, neutrons leave only a shower in the HCAL.

The photons are stopped by the ECAL. They are all absorbed and leave generally no track in the inner detector. The electrons are also stopped by the ECAL, but they leave a clear track in the inner detector. From the track and with its curvature the transverse momentum can be measured as well as the charge allowing to distinguish electrons and positrons.

The muons are the only charged particles which can leave the detector without interfering with the inner detector. This is because they don't interact strongly, so they very rarely undergo hard collisions with atomic nuclei, where they could lose significant energy. They do interact electromagnetically, so they collide with electrons, but because they are much heavier than electrons, they only lose a small fraction of energy in those collisions. So they are only identified with the tracks in the inner detector and the muon spectrometer. Also, the use of the track curvature is used to differentiate between muons and antimuons.

The taus mainly decay into hadrons and with about 1/3 of probability it decays into an electron or a muon (positron or an antimuon for the antitau). Requiring a low track multiplicity and a narrow cone of the jet it is possible to identify them.

The neutrinos are not possible to detect directly with ATLAS because they interact weakly. However, knowing that the initial total energy and momentum in the transverse plane is zero, it is possible to identify the neutrinos by reconstructing all the other particles resulting from the hard-scatter collision.. For this the missing transverse momentum E_T^{miss} is used. The E_T^{miss} is also an important quantity to identify the possible production of dark matter candidates produced by the LHC collisions.

Since we are colliding hadronic particles (i.e. protons), quarks and gluons are produced in abundance. They hadronise in the detector and leave multiple tracks in the inner detector. They are look at as jets, which are objects reconstructed with jet algorithms like the anti-k_t algorithm (Section 3.2.1).

The hadrons originating from a bottom quark travel some distance and decay into a jet after. This is because bottom hadrons have a relatively long lifetime of 1.5×10^{-12} s. This produces a track in the b-jet from a secondary vertex which is slightly displaced with respect to the primary interaction. This is used in the b-tagging, which identifies jets coming from a b-quark so-called b-jets. [38]

Chapter 3

Jets

3.1 Introduction

During a high-energy proton proton collision multiple quarks and gluons are produced. As quarks and gluons cannot exist in isolation (QCD confinement) they cannot be directly observed as single particles and they recombine spontaneously with other quarks to form hadrons. This is called hadronisation. As result from this process different colourless objects are created. A jet is a collimated spray of hadrons and other particles and it represents hadronic showers at the detector. An example is an event with 6 jets coming from original top and anti-top quarks, which decay into two vector bosons W and into a bottom and anti-bottom quarks. What is observed at the detector is six jets coming from the resulting bottom and anti-bottom quarks and the decay of the two vector bosons.

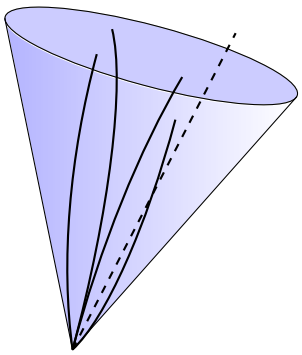

FIGURE 3.1: Sketch of a jet.

When the vector boson is produced with a transverse momentum much larger than its mass, the resulting jet is called boosted. Products from this decay are very collimated and so they can be confined into a single larger jet (Figure 3.2), composed of subjets.

Two typical size of jets are reconstructed by the jet algorithm. For the resolved jets, the typical size is of $R = 0.4$, where R is the jet radius parameter used by the algorithm to define the final size of the jet. Those jets are called small-R jets. Boosted jets can have size of $R = 1$ and they are generally called large-R jets. Because the two showers overlap, it is better to reconstruct them as a single large radius jet to make sure that all the energies deposited from the hadronic decays are caught.

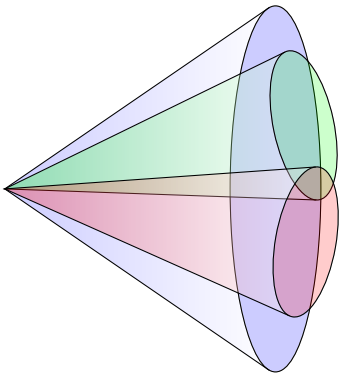

FIGURE 3.2: Sketch of a boosted jet.

3.2 Jet reconstruction

Jets can be reconstructed from the information that is available at the detector. They can be reconstructed from different constituents : topological clusters, particle flow objects (discussed latter), tracks, etc. ATLAS uses information from topological clusters. So the inputs to reconstruct the jets are the topological clusters (topo-clusters) of the calorimeter signals. This calorimeter algorithm is discussed at section 4.4.1 .

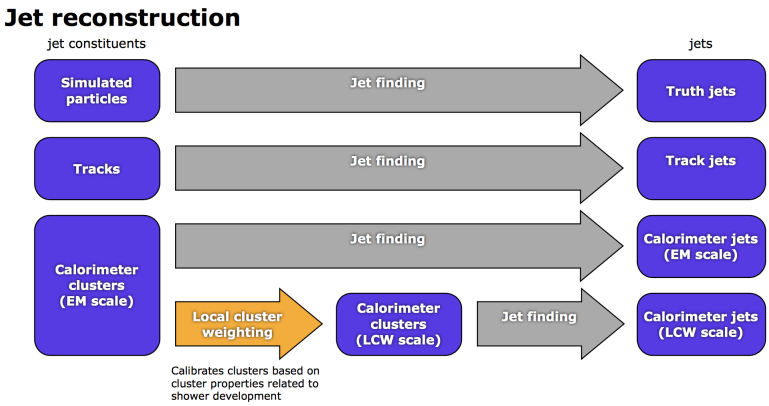

FIGURE 3.3: ATLAS jet reconstruction.[4]

Topo-clusters can be either calibrated at the electromagnetic scale where the energy of an isolated topo-cluster is the sum of its constituent cell energies or at the local cell weighting scale where this scale accounts for the difference between electromagnetic and hadronic interactions in the ATLAS calorimeters.

3.2.1 Jet Algorithms

The primary algorithm that uses ATLAS to perform jet reconstruction is called the anti-k_t algorithm. This algorithm contributes dictate how particles should be grouped together to form jets. Good jets reconstruction algorithms should guarantee both infrared and collinear safety. Infrared safe means that the presence or absence of additional soft particle which are particles having a low p_T compared to the mean

interaction with the highest p_T, should not modify the result of jet finding, for instance the number of jets. For the case of collinear safe, jets should not be sensitive to particles radiated at very small angle.

There are two classes of algorithms: cone algorithms and successive recombination algorithms. The cone algorithm is employed before data taking and starts from jet inputs with energy above a certain threshold and sums the four-momenta of all particles in a surrounding cone in the $\eta - \phi$ space with radius R. This algorithm does not well behave perfectly so the jet algorithm employed in ATLAS is the anti-k_t algorithm. This algorithm is a successive recombination algorithm and is part of a set of k_t algorithms. The sequential reconstruction algorithms are algorithms where the inputs of the reconstruction (topological clusters, particle flow objets, tracks, and so on) depend on their distance to each other, combining two particles together at each step. The algorithm uses two distances:

$$d_{ij} = min(p_{ti}^{2p}, p_{tj}^{2p}) \frac{\Delta_{ij}^2}{R^2} \tag{3.1}$$

$$d_{iB} = p_{ti}^{2p} \tag{3.2}$$

where $\Delta_{ij}^2 = (y_i - y_j)^2 + (\phi_i - \phi_j)^2$ and p_{ti}, y_i and ϕ_i are the transverse momentum, rapidity and the azimuth angle respectively from the particle i. R is the radius parameter that enters in the jet definition regulating the size of the jets and an additional parameter p which defines how the characteristics of the entities are combined. The distance d_{ij} is the distance between the particles i and j and d_{iB} is the distance between the entity i and the beam (B). The algorithm works as follow : it computes all the distances d_{ij} and d_{iB}, and identifies the smallest distance. If the smallest distance between all d_{ij} and d_{iB} is d_{ij} ($d_{ij} < d_{iB}$) then particles i and j are combined otherwise ($d_{iB} < d_{ij}$) the entity i is considered a jet and not considered in the next iteration. The algorithm continues until no input is left. The different k_t algorithms depend on the value taken by the parameter p. For $p = 1$ it is the k_t algorithm, for $p = 0$ it is Cambridge/Aachen (C/A) algorithm and for the $p = -1$ it is the anti-k_t algorithm.[22]

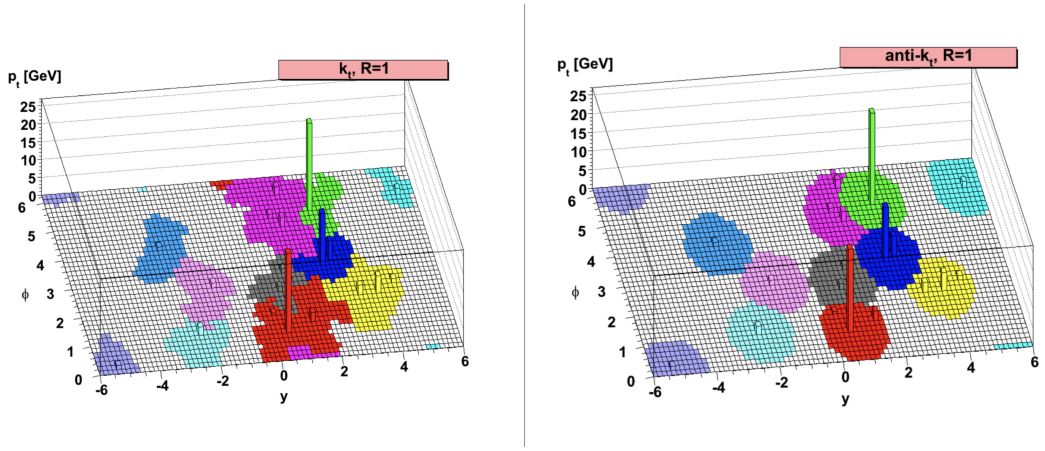

FIGURE 3.4: Simulation of different jets algorithms.[22]

The anti-k_t algorithm can be understood as followed. Considering a collision event providing with a few well separated particles with large p_T and with many

particles with a small p_T. The distance d_{1j} (eq. 3.1) between a particle 1 with a large p_T and particles j with a small p_T is exclusively determined by the transverse momentum of the particle with the large p_T and the separation Δ_{1j}. But the distance between two separated particles with a small p_T will be much larger. So the particles not having a very large p_T tend to cluster faster with the particles with large p_T before clustering with each other. If the large p_T particles have no neighbours like them within a distance $2R$ then it accumulates the smaller p_T particles within a circle of radius R, giving a perfectly circular cone-shaped jet.[22]

If two particles of large p_T are present such that their distance between them Δ_{12} follows the condition $R < \Delta_{12} < 2R$, two jets will be formed. The shapes for both do not always follow a perfectly cone shape. This is because if the p_T of the particle is much larger then the other, the jet of the highest p_T particle will be conical and the other jet will be partly conical, since it will miss the part overlapping. If they have the same transverse momentum neither jet will be conical and the overlapping part will simply be divided by a straight line equally between the two. Same goes for the case when $\Delta_{12} < R$. The two particles will in this case form a single jet. If the p_T of one of the two particles is larger than the other then it will create a conical jet centred on that particle with the larger p_T. If the p_T of both are approximatively the same the shape will instead be more complex, being the union of cones around each particle with large p_T with additionally a cone centred on the final jet. So the main ideas to get from this is that the particles with a small p_T do not modify the shape of the jet instead of the ones with a large p_T. The jet boundary in this algorithm is resilient with respect to the radiation of particles with small p_T but sensitive with respect to the radiation coming from large p_T particles.[22]

The behaviours of two different jet algorithms are shown in figure 3.4. It can be seen that the anti-k_t algorithm gives a much more regular circular shapes making it easier to compute areas. The anti-k_t algorithm immediately clusters the particles with small p_T to the ones with a large p_T and so no substructure information can be obtained. The other algorithm, k_t algorithm goes back the showering process and therefore substructure information can be obtained.

3.3 Jet calibration

After building jets, they have to be calibrated to account for several effects. The calibration consists of the following steps . First, interactions with lower energies are suppressed (pile-up), then the jet is calibrated to the Monte Carlo truth scale, and at the end the difference between MC and data are taken into account. The calibration chain is different for the two typical size of jets (figure 3.5). The following explanations for the three steps uses the references [30], [43], [21].

3.3.1 Pile-up correction

At the LHC, an event is a collision between opposing proton bunches. The rate of these events is 40MHz. The collisions between protons induce inelastic interactions. For one event, the most energetic proton-proton interaction in one bunch crossing is called the hard scatter interaction. The hard scatter interaction is not the only interaction happening. It goes along with other interactions with lower energies, called

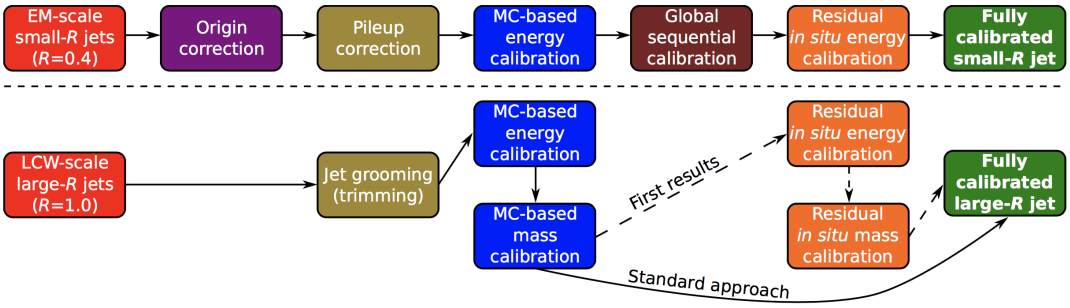

FIGURE 3.5: An overview of the calibration chain for both small-R and large-R jets is shown.[43]

the pile-up interactions (figure 3.6). During the reconstruction with the help of the jet algorithms, these particles coming from the pile-up interactions might be taken into account in the clustering inside a jet. The pile-up can alternate the properties of the constructed jets. To suppress as much as possible different techniques are used depending in the size of the jets (more in section 3.5).

Large-R jets

For the large-R jets the effect of pile-up is increased due to the larger fraction of the calorimeter enclosed within the jet volume. Therefore the large-R jets are usually groomed using techniques called grooming techniques, that suppress pile-up effects. Grooming is a class of algorithms that throw away constituents of a jet following a defined strategy and rebuild the jet from the remaining constituents. ATLAS usually uses the trimming procedure. This procedure consists of taking the original jet from the anti-k_t algorithm, re-clusters the constituents in it using the k_t algorithm with a certain distance parameter and throwing away constituents in a given sub-jet if the p_T of the sub-jet is less than a certain fraction of the large-R jet p_T.

Small-R jets

In comparison to the large-R jets, the small-R jets comes with a origin correction. This correction forces the jet axis to point to the hard-scatter vertex of interest. At the event by event level, the energy density is calculated to have an idea on the global pile-up energy present in a given event. This is used together with the area of the jet [21] to evaluate for each individual jet a measure of the local size of the jet. The energy from this local size jet is subtracted from the original jet to remove the pile-up energy contributions. There is also residual corrections which removes the remaining dependence of the jet on the number of reconstructed primary vertices and the expected average number of interactions per bunch crossing. These residual corrections are especially used at the region $|\eta| > 2$ because the energy density is not calculated in that region.

3.3.2 MC-based calibration

After the pile-up correction, the jets are calibrated using the MC information. A large fraction of the energy in a hadronic shower is not taken into account in the detector because of some parts are inactive for detection. The energy needs to be recovered

to measure precisely the Jet Energy Scale (JES). To do so a MC simulation can be done, comparing reconstructed jets to jets built from simulated particles, defined as the truth jets. The correction of the lost energy can be applied calibrating the average reconstructed jet to the truth scale by defining the response $X_{reconstructed}/X_{truth}$. The same approach is used for both small-R and large-R jets. An additional step can be done for the large-R jets calibrating on a well defined mass as they are used to represent the hadronic decay of a massive particle. For this a mass response instead of an energy response is defined.

The JES for the small-R jets is even more improved by applying what is called the Global Sequential Calibration (GSC). This is uses to improve further the jet responses for properties related to shower development, flavour differences and jets which are not fully contained by the calorimeters.

3.3.3 Residual *in situ* calibration

Following the MC-based calibration, is when the JES calibration is applied to jets measured in data. These are data derived calibrations and any differences from data can lead to biases in the jet energy and mass. It is done by calculating the jet response difference between data and MC simulation using the transverse momentum of a jet and a well-measured reference object.

3.4 Particle Flow

Particle flow is a hadronic reconstruction algorithm that combines information from the inner detector and the calorimeter. It uses the topo-clusters as the previous algorithm but also the track information. The algorithm matches the tracks to the energies of the topo-clusters in the calorimeter to produce charged particle flow objects. The algorithm aims to take full advantage of all the particle detectors subsystems to improve the energy resolution of reconstructed physics objects and is particular interest to SUSY analyses. This is because it has the potential to improve the jet energy resolution, and therefore, the E_T^{miss} resolution as well.

More precisely, the use of particle flow has the advantage that at low energy the tracking detectors provide a better p_T resolution for charged particles than the calorimeters. The algorithm has four main stages. First, the track-cluster matching where the tracks from charged particles in the tracking detector are extrapolated to the calorimeters. Then comes the removal of energy from calorimeter cell deposits from the clusters with associated tracks from the tracking detectors which is called the charged fraction subtraction. This step removes the double counting of energy already deposited by the charged particles in the calorimeters. And finally the calibration of neutral particles. [1]

The ATLAS particle flow algorithm works as followed. First, tracks are selected following well-defined criteria. The algorithm tries to match each track to a single topo-cluster in the calorimeter. For this, the distances $\Delta\phi$ and $\Delta\eta$ between the barycentre of the topo-cluster and the track are used. The expected energy deposit of the particle in the calorimeter that also created the track is computed based on the topo-cluster position and the track momentum. A single particle can deposit energy in multiple topo-clusters. For each track and topo-cluster matching set, the algorithm evaluates if it is necessary to add more topo-clusters to recover the full

shower energy. The expected energy deposited in the calorimeter by the particle that produced the track is them subtracted in the calorimeter. The subtraction is done cell by cell from the set of matched topo-clusters. At the end, if the remaining energy in the system is coherent with the expected shower fluctuations of a single particle signal, the topo-cluster remains are removed. This results with the track of a charged particle. So there are three outcomes of this algorithm : charged particle tracks, topo-clusters which have not been modified by the algorithm because there where not matched to tracks and modified topo-clusters which had remain part of their energy removed. [1]

3.5 Pile-up suppression

There exist two types of pile-up : in-time pile-up and out-of-time pile-up. In-time pile-up interactions arise from additional proton-proton interactions in the current bunch crossing whereas out-of-time pile-up refers to energy deposits at the ATLAS calorimeter from previous and following bunch crossings relative to the triggered event. In other words, out-of-time pile-up relates to the time required for the signals coming from residual energies, to develop and to be read by the detector from previous or future bunch crossings.

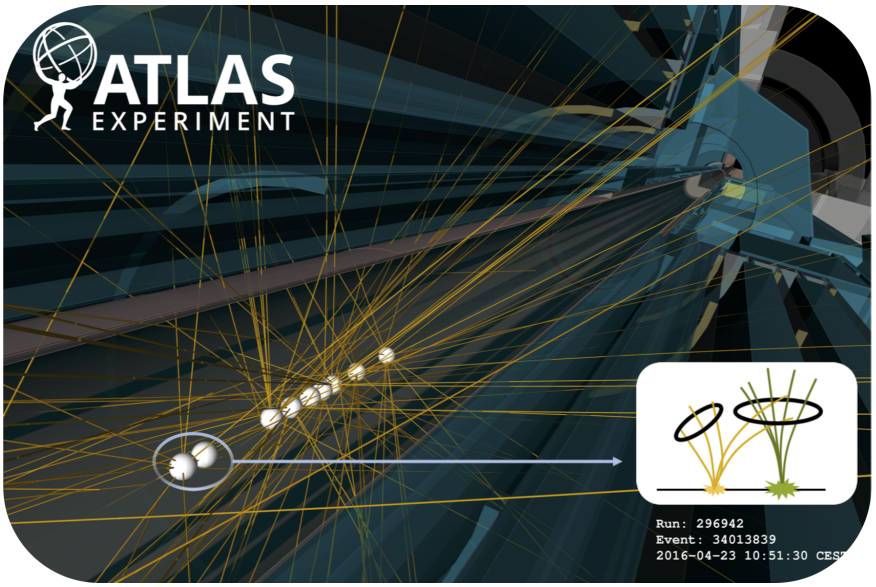

FIGURE 3.6: Simulation ATLAS Events at 13 TeV - First 2016 Stable Beams. [17]

As mentioned previously, in-time pile-up is the phenomenon where multiple collisions happen in a single crossing. Increasing the number of protons per bunch or reducing the beam size leads to an increase to the number of simultaneous collisions, and thus the in-time pile-up. Pile-up is parametrised in terms of the number of reconstructed primary vertices N_{PV} for in-time pile-up and in terms of the average number of proton-proton inelastic interactions per bunch crossing $\langle\mu\rangle$ for out-of-time pile-up. N_{PV} is related to the number of reconstructed primary vertices in the tracking detector per event (figure 3.7). $\langle\mu\rangle$ is an average over events and is related

to the instantaneous luminosity [28]:

$$\langle \mu \rangle = \frac{L \times \sigma_{inel.}}{N_{bunches} \times f_{LHC}} \tag{3.3}$$

where L is the instantaneous luminosity, $\sigma_{inel.}$ is the total inelastic proton-proton cross-section and $N_{bunches} \times f_{LHC}$ is the average frequency of bunch crossings in the LHC. The instantaneous luminosity reaches $5 \times 10^{33} cm^{-2} s^{-1}$ and the average pile-up goes beyond 50 interactions per bunch crossing.

The effect of pile-up is not to be overlooked. When it comes to the reconstruction and the calibration of the jets from calorimeter signals, the effect of pile-up is particularly important. The particles originating from pile-up interactions can overlap with the jet originating from the hard scatter interaction and affect the reconstructed jet kinematics (3.6). Also the pile-up gives additional jets to any event.

To produce robust results, the pile-up must be suppressed as much as possible. The pile-up is affecting both the trigger and the offline reconstructed jets. An efficient way to suppress pile-up is to perform an average correction parametrised by N_{PV} and $\langle \mu \rangle$ (Section 3.3.1). These corrections can be enhanced by the addition of tracking information. At the trigger level, tracks will be provided by FTK so these may be used to further reject any jets not originating from the hard-scatter interaction.

3.5.1 The jet vertex tagger

To look if the vertex comes from a hard-scatter interaction or not, the jet vertex fraction (JVF) is adopted. For a given jet, the JVF identifies the origin of the jet and tells if it comes from pile-up or not. Using the JVF variable can, in other words, help to filter the jets coming from the collision between opposing proton bunches.

The JVF variable is defined for each jet with respect to each identified primary vertex in the event. The identification of the primary vertex is done by looking at the origin of the charged particle tracks pointing towards the given jet. So the primary vertex is, in other words, the origin where the proton-proton interaction happened. The primary vertex with the highest $\sum p_T^2$ of constituent tracks is chosen to correspond to the so called hard-scatter vertex, the one originating from the the hard-scatter interaction. Once the identification of all the primary vertices of the event is done, the JVF can be used to select jets having a high likelihood to originate from hard-scatter vertex. The JVF is defined as in equation 5.2. [28]

$$JVF = \frac{\sum_k p_T^{trk_k}(PV_0)}{\sum_l p_T^{trk_l}(PV_0) + \sum_{n \geq 1} \sum_l p_T^{trk_l}(PV_n)} \tag{3.4}$$

The different terms can be explained as follow. The PV_0 is the primary vertex of the hard scatter interaction and $PV_{n \geq 1}$ corresponds to the primary vertices due to the pile-up interactions in the same event. The JVF variable can have the values between 0 and 1 and for jets with no associated tracks the value -1 is adopted. When the value for the JVF is 1 then this indicates that all the tracks associated to the jet originate from the hard scatter interaction. On the contrary, when the the value for the JVF is 0 for a jet, this indicates that all associated tracks originate from pile-up vertices. The values between 0 and 1 indicate that some tracks originate from the

hard-scatter vertex, while others come from pile-up. So the JVF gives the fractional p_T from tracks associated to the hard scatter vertex.

The denominator in the formula (5.2) is in function of the number of reconstructed primary vertices (N_{PV}) in the event. An increase of N_{PV} is explained by the fact that the number of pile-up tracks associated with the jet increases. So as the denominator of JVF increases with N_{PV}, the mean JVF is shifted to smaller values. This can be seen by the figure 3.7 from [29]. So JVF explicitly depends on the pile-up. This also results that the jet efficiency when imposing a JVF criterion to reject pile-up, depends on N_{PV}. To resolve this, a new track based variable is developed to suppress pile-up jets keeping the efficiency stable as a function of N_{PV}.

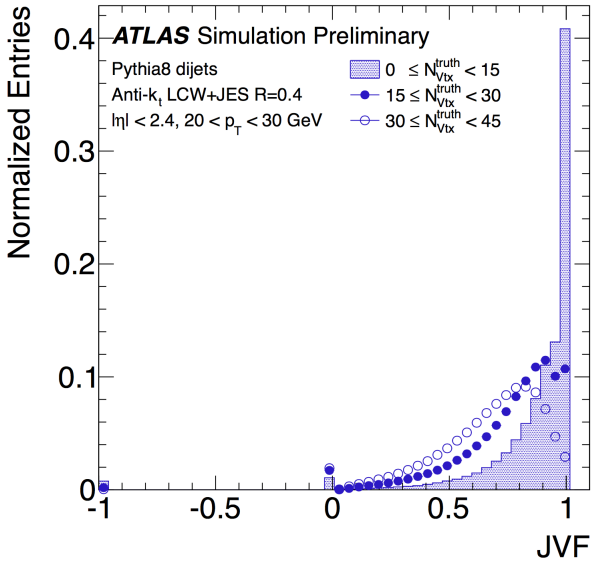

FIGURE 3.7: The JVF distribution for hard-scatter jets in simulated dijet events for different bins in truth vertex multiplicity $N^{truth}_{Vtx} = N^{truth}_{PV}$. [29]

The jet-vertex-tagger or JVT is the successor of the JVF. It is a improvement of the older variable JVF in terms of pile-up dependence. JVT variable is the variable of our interest in this thesis and will be used to suppress pile-up. It has the same origin than the JVF and so is used in the same way, meaning that fixing a criterion on it, it gives a method to separate hard scatter jets from the pile-up jets. Basically, it is the JVF variable but corrected to be as much as possible independent to the pile-up.

The jet vertex tagger is developed from the combination of two jet variables [25] : $corrJVF$ and R^0_{pT}. The $corrJVT$ is defined as follow:

$$corrJVF = \frac{\sum_k p_T^{trk_k}(PV_0)}{\sum_l p_T^{trk_l}(PV_0) + \frac{\sum_{n\geq 1}\sum_l p_T^{trk_l}(PV_n)}{(k \cdot n_{trk}^{PU})}} \tag{3.5}$$

where, as before, PV_0 is the identified hard scatter vertex and $PV_{n\geq 1}$ is the primary vertices due to the pile-up interactions. The term $\sum_l p_T^{trk_l}(PV_0)$ is again the scalar p_T sum of the tracks associated with the jet originated from the hard scatter vertex and the term $\sum_{n\geq 1}\sum_l p_T^{trk_l}(PV_n) = P_T^{PU}$ is the scalar p_T sum of the tracks associated

with the jet originated from the pile-up vertices. But a change from the previous definition of the JVF occurs : the P_T^{PU} is divided by $(k \cdot n_{trk}^{PU})$, with n_{trk}^{PU} the total number of pile-up tracks per event. This is done to correct the linear increase of P_T^{PU} with the pile-up. The parameter k is set to 0.01 [26].

The other variable used by JVT is R_{pT}^0. It is defined as follow :

$$R_{pT}^0 = \frac{\sum p_T^{trk}(PV_0)}{p_T^{jet}} \tag{3.6}$$

It is the scalar p_T sum of the tracks that are associated with the jet and originated from the hard scatter vertex divided by the calibrated jet p_T which includes pile-up subtraction (Section 3.3.1). It looks at the similarity between the jet p_T and the total p_T of the hard scatter charged particles within the jet. The numerator does not takes into account the trackless particles, in other words the neutral particles.

With those two variables the JVT can be constructed as a 2D likelihood from $corrJVF$ and R_{pT}^0. To do this, the nearest neighbour algorithm [12] is used to avoid statistical fluctuations. The JVT variable is the variable that is used in the further studies in this thesis.

Chapter 4

The ATLAS trigger system

4.1 Introduction

The main focus of this thesis is on the ATLAS trigger system. This system is crucial for the experiment, it is responsible for selecting the events of interest. For a given bunch crossing interaction the system will decide whether or not to keep the event. There is about 40 million particle collisions per second happening at the detector. It would be impossible for the readout and the storage to record all the collisions at the detector. Also all the events are not relevant for the interesting physics so the trigger system selects only the events which are interesting and so record less events. A good and reliable trigger and data acquisition is required to be as stable as possible.

4.2 The Trigger system

The ATLAS Trigger system has to deal with the event rate from the LHC bunch crossing rate of up to 40 MHz. To store only the relevant data, the trigger has to reduce the rate by selecting the interesting events. A two-level trigger system is used in the ATLAS experiment :

- Level 1 (L1) : a hardware based system, which reduces the rate from 40MHz to approximatively 100kHz. It makes decisions within the 2.5 μs based on information of the muon and the calorimeter systems.
- High Level Trigger (HLT) : a software based system which receives informations from L1 for specific regions and can be used for reconstructions at particular regions in the trigger algorithms. It reduces the rate of around 100kHz at the end of L1 to approximatively 1kHz.

As said before, compared to the LHC Run1 there was an increase of centre-of-mass energy from 8 TeV to 13 TeV at the Run2. This increase of energy with a higher luminosity leads to higher pile-up and an increase of rates compared with the Run1 trigger system.

That can be explained by a series of reasons. One of them is the fact that the increase of centre-of-mass energy is accompanied with a decrease of the bunch spacing from 50 *ns* to 25 *ns*. The increase of energy gives on average 2 to 2.5 times larger trigger rates even though the beam size and the bunch population was lower than in Run1. But also, the decrease of bunch spacing increases certain trigger rates coming from additional interactions from neighbouring bunch-crossings. The LS1 was therefore used for a major upgrade of the trigger system. Seen in figure 4.1 is the trigger system used for the Run2.

For the Run3, the LHC will have approximatively the same luminosity as the Run2 but new improvements at the trigger level will be present. A new hardware

at the trigger, FTK (Fast Tracker) gives rise for improvements at the trigger selection and will open up new perspectives. The pile-up of about 60 proton-proton interactions is already known from the Run2 but further developments is done for the Run3 to gain a significant amount of pile-up suppression. Thanks to FTK, track information will be implemented. This is crucial to distinguish primary vertices from pile-up. Therefore, FTK provides a full-event tracking and so the HLT jets of Run3 will be better than the HLT of Run2.

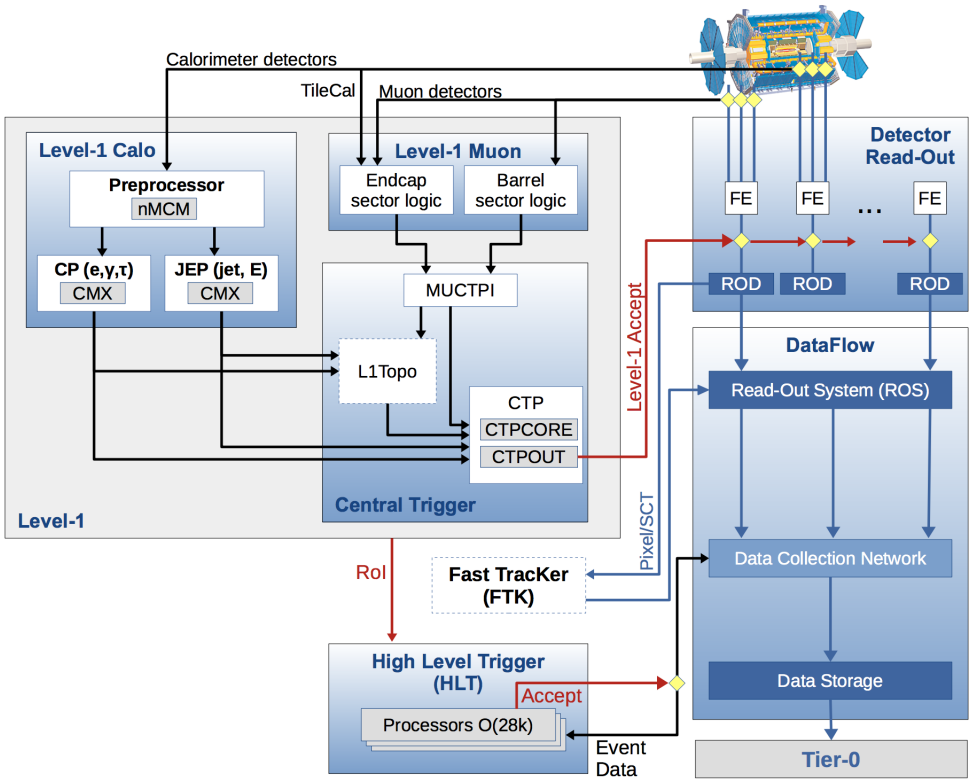

FIGURE 4.1: Schematic layout of the ATLAS trigger and data acquisition system [27]

4.3 The Level 1 Trigger system

The Level 1 trigger is the first step to reduce the rate and so to select the interesting events. To separate the desired processes from the predominant jet production and pileup, L1 searches for exclusive signatures that could identify high transverse-energy electrons, photons, muons, tau's and jets with a high total transverse energy. The main goal is to be able to do this in a fast way. Therefore, L1 uses reduced-granularity data from the muon and calorimetric detectors. The granularity of data means the level of detail considered in a model or decision making process such as the trigger in this case. The greater the granularity, the deeper the level of detail and vice-versa. The two detectors are used for the following signatures :

- using the resistive-plate chambers (barrel) and thin-gap chambers (endcap) of the muon detector for muons

- and using all of the calorimeters for electromagnetic clusters (electrons and photons), jets, tau's decaying into hadrons and missing and total transverse energy.

As mentioned before the maximum rate is of approximatively 100kHz. The time interval between two bunches is about 25 ns and this is too short for processing and selecting events. So to be able for the L1 to work properly the detector data is held in buffers. In other words the data is temporarily stored while L1 makes its decisions. If the bunch-crossing passes the L1 criteria, a L1 Accept signal is sent and the data are kept, if not they are deleted. The accepted events are then passed to the High Level Trigger. The time allowed for the L1 stage depends on the size of the buffers. And so the allowed decision time, or latency, for L1 is of 2.5 μs as already mentioned. An interesting note: of that time, a large fraction is spent by the signal transmission from and back to the detector front-end electronics.

So the Level 1 trigger consists of three main parts: the L1 calorimeter trigger system, the L1 muon trigger system and the Central Trigger. The L1 calorimeter system and the L1 muon system provides trigger information to the Central Trigger.

4.3.1 Level-1 calorimeter trigger

The Level-1 calorimeter trigger in simple words, reconstructs energy depositions in the calorimeters. For this, different algorithms are used for the different signatures interested. The High Level Triggers receives what is called Regions-of-Interest (RoI's) information from L1. These are regions of the detector where the L1 trigger has identified possible trigger objects within the event. This is used for regional reconstruction in the trigger algorithms. The Level-1 calorimeter identifies those RoI's with the different trigger algorithms.

The are three main parts in the level-1 calorimeter trigger are : the preprocessor, the Cluster Processor (CP) and the Jet/Energy-sum Processor (JEP). Firstly, the Preprocessor system is used to serve as a digital signal source for the subsequent processors. It digitises and calibrates the analogue input signals coming from the calorimeter detectors. The Preprocessor system also performs an important operation called Bunch Crossing Identification (BCID), which is there for associating a signal with a particular LHC bunch crossing. It serves as input for the CP and the JEP.

The CP identifies electron/photon and tau lepton candidates with transverse energy above a certain threshold and if necessary a certain isolation criteria. This is achieved by performing a so called sliding window algorithm of 4×4 trigger towers, seen in figure 4.2. One trigger tower has the dimensions in the $\eta - \phi$ space of $\Delta\eta \times \Delta\phi = 0.1 \times 0.1$ in most parts, but larger at higher $|\eta|$. This algorithm identifies a RoI as a 2×2 trigger tower cluster in the electromagnetic calorimeter. Those RoI's are summed across both the electromagnetic and hadronic calorimeter layers and are found to be a local maxima in transverse energy compared to their nearest neighbours. Because of this, the identified candidates are not counted multiple times. In the case for electrons and photons the most energetic of the horizontal or vertical (1×2 or 2×1) cluster sums in the electromagnetic layer must be greater than a predefined threshold. To discriminate between single objects and broader hadronic jets a certain isolation requirement is used. This requirement states that an

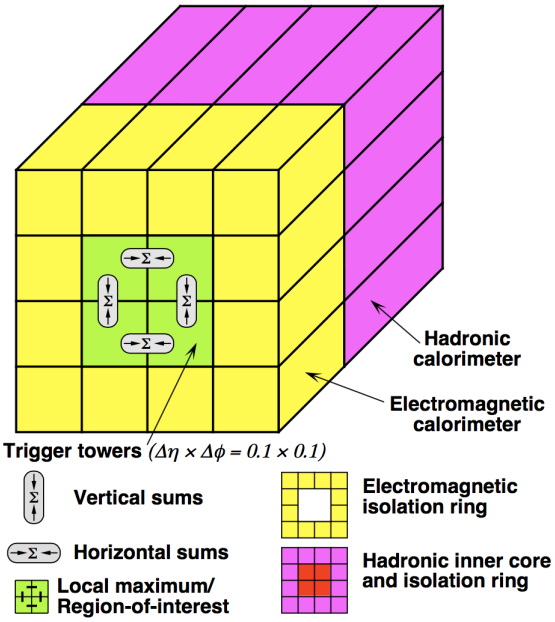

FIGURE 4.2: Schematic view of the trigger towers used as input to the L1Calo trigger algorithms. [29]

electromagnetic isolation ring and a hadronic ring must be less than a corresponding predefined threshold in transverse energy. In order to correct the different energy responses of the detector, the energy threshold can be set differently for different $|\eta|$ regions with a granularity of 0.1 in $|\eta|$. The uses of the hadronic core is to identify tau lepton candidates. This combined with the EM cluster sum gives the possibility to identify tau lepton candidates and so the hadronic core isolation requirement is removed. The algorithms are processed by four crates of electronics each operating in one quadrant in of the calorimeter. Those crates contain 15 Cluster Processor Modules and each of them scans a core region of 16×4 trigger towers.

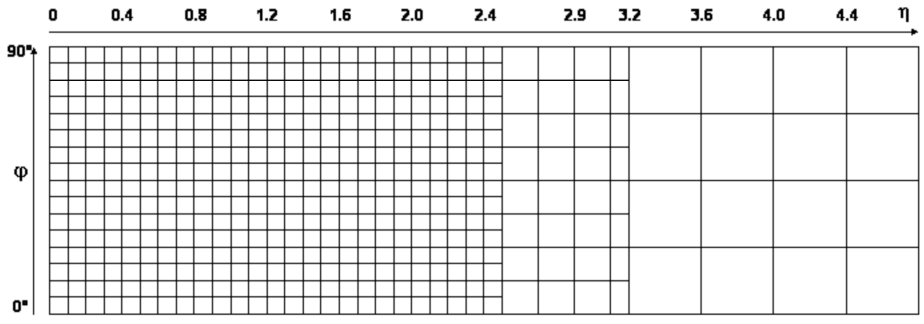

FIGURE 4.3: Trigger-tower granularity for $\eta > 0$ and one quadrant in ϕ. [9]

The JEP is a processor which identify jets as well as calculate the missing transverse energy and the total transverse energy. The used algorithms processes jet elements that are the sum of 2×2 trigger towers in the EM calorimeters added to 2×2 trigger towers in the hadronic calorimeters, giving a basic granularity of 0.2

in $\Delta\phi$ and $\Delta\eta$. Like the sliding window algorithm implemented in the CP, the jet algorithm identifies local energy maxima RoIs of 2×2 jet elements in size. Like seen at figure 4.4. It calculates cluster sums of 2×2, 3×3 or 4×4 of jet elements size windows. Those sums are then compared to jet transverse energy thresholds which are different for each of the cluster sizes. The algorithm covers $|\eta| < 4.9$ but in the forward region ($3.2 < |\eta| < 4.9$) the jet elements are treated differently because the granularity is much coarser in both $|\eta|$ and ϕ (figure 4.3). So jets who are triggered in the forward region are less reliable and susceptible to pile-up. The algorithms of the JEP is contained in two crates consisting of 16 Jet/Energy-sum Modules each that handle two opposite quadrants in ϕ. Each module processes an area of 8×4 jet elements in size and calculates sums of the transverse energy within $|\eta| < 4.9$.

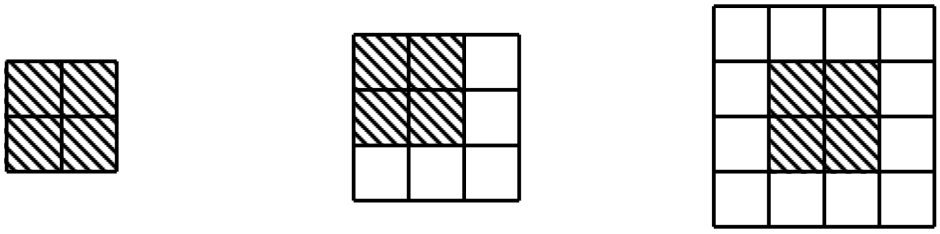

FIGURE 4.4: Operating the jet algorithm on jet elements indicated by the 0.2×0.2 in size of the grid (one square of the grid). Three transverse energy cluster sizes of jet elements are shown with the corresponding RoIs in the shaded squares. [9]

The outputs of the CP and JEP modules are Trigger Objects (TOBs) with information on the location, the transverse energy and type of object identified. The modules send those TOB's to the L1 Topological trigger modules which forms combined trigger objects, based on full event topology. After the L1 Topological modules, those TOBs are send to the CTP. Using a module called Common Merger module eXtended (CMX) the counts of objects over a certain threshold are also send to the Central Trigger Processor (figure 4.1) and provides RoI's and read-out data to the HLT. [6]

4.3.2 Level-1 muon trigger

The Level-1 muon trigger is responsible for the muon triggers. Muon triggers are based on the information provided by the muon spectrometer (MS) and the inner detector (ID) of the ATLAS detector (more in section 2). This level-1 muon trigger system identifies muons by spatial and temporal coincidence requirements on the hits provided by the resistive plate chambers (RPC) and the thin gap chambers (TGC) of the muon system (Section 2). A estimation of the muon candidates transverse momentum thresholds at L1 is done by taking the degree of deviation from a hit pattern set by an infinite momentum assumption. At the barrel region where the RPC are located ($|\eta| < 1.05$), the size of the Regions-of-Interest are 0.1×0.1 in the $\eta - \phi$ space. The requirement in the RPC is that a coincidence of hits in the three layers for the highest three p_T thresholds is needed, while for the remaining lower p_T thresholds the hit requirement is set to two coincidence hits at the layers (figure 4.6). For the endcap regions where the TGC are located ($1.05 < |\eta| < 2.4$), the coincidence in three layers is required for all thresholds. The Regions-of-Interest are then to the Central Trigger Processor.

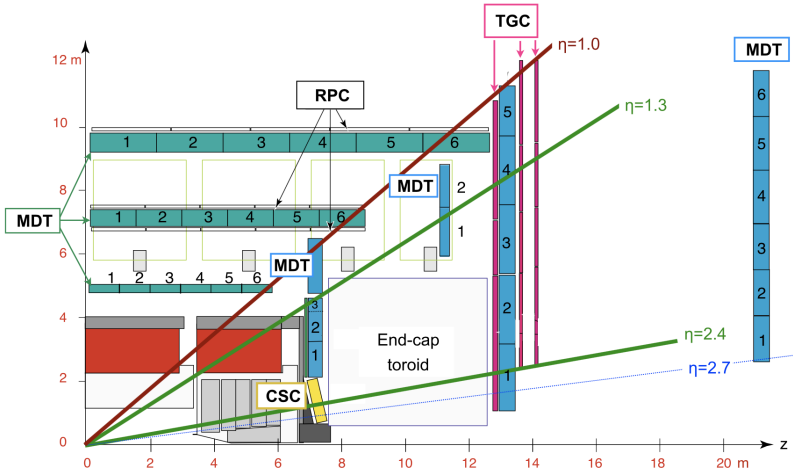

FIGURE 4.5: Schematic picture showing a quarter-section of the muon system in a plane containing the beam axis, with drift tube (MDT) and cathode strip (CSC) chambers for momentum determination and resistive plate (RPC) and thin gap (TGC) chambers for triggering. [5]

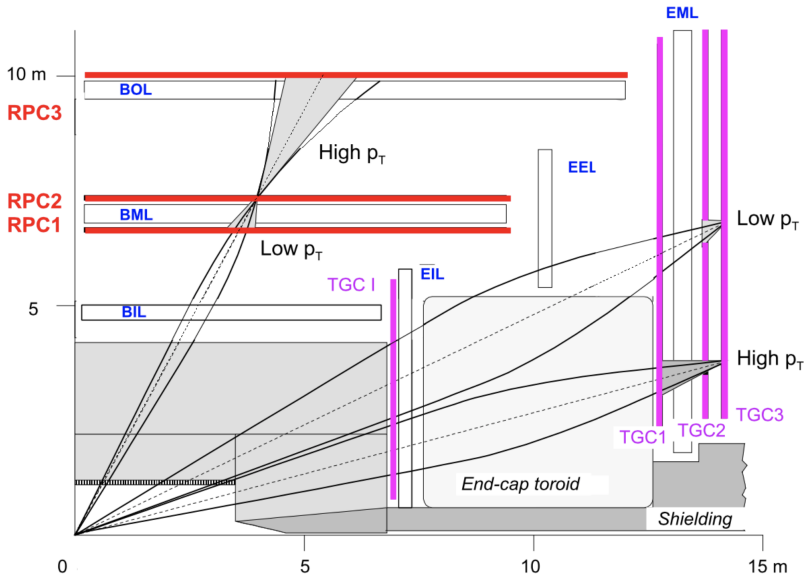

FIGURE 4.6: Schematic picture showing a quarter-section of the muon system with the hits for the different p_T thresholds. [5]

4.3.3 Central Trigger

The first part of the Central trigger consists of L1 Topological trigger modules (L1Topo), a Muon-to-CTP interface (MUCTPI) and the Central Trigger Processor (CTP).

The L1 Topological trigger modules are newly introduced at the Run 2 and has 2 FPGAs (Field-Programmable Gate Array) per module. Their job is to calculate physical variables in the interval time of 2 μs with the information of the L1 calorimeter system and the L1 muon system. Those variables calculated with algorithms, allows the Central Trigger Processor to perform Level 1 selections. Typical examples of such quantities are angular separations for better signal-to-background separation,

global quantities like H_T which are sums of the E_T of jets for fat jets identification. Also an other example of a variable of interest is ΔR which is the separation of two jets in the η - ϕ space of the detector. So those Topological trigger modules combine information from the L1 calorimeter system and the L1 muon system into variables that are used for additional L1 selections (topological). This is useful for final states with E_T^{miss} like Higgs decays for example.

The Muon-to-CTP interface (MUCTPI) is located between the L1 muon trigger system and the Central Trigger Processor (CTP). This interface receives muon candidates information from the L1 muon trigger system. He counts the muon candidates for each transverse momentum (p_T) threshold and sends the result to the Central Trigger Processor (CTP). In other words, it sends the multiplicity of muon candidates to the CTP. The interface takes in this way into account for the possible double counting of muons. This double counting can be detected by more than one muon sector due to geometrical overlap of the muon chambers and the trajectory of the muon in the magnetic field. The interface sends muon candidate information alongside to the CTP, also to the L1 Topological trigger.

The Central Trigger Processor is one of the key elements of the Level 1 Trigger system. It is this element who makes the L1 trigger decisions to the L1 inputs. It receives all the trigger information such as multiplicities for electrons/photons, taus/hadrons, jets, and muons as well as flags for total transverse energy, total missing energy and total jet transverse energy. This is then used to make the final trigger decision (L1 Accept) on the basis of lists of selection criteria, which is called the trigger menus.

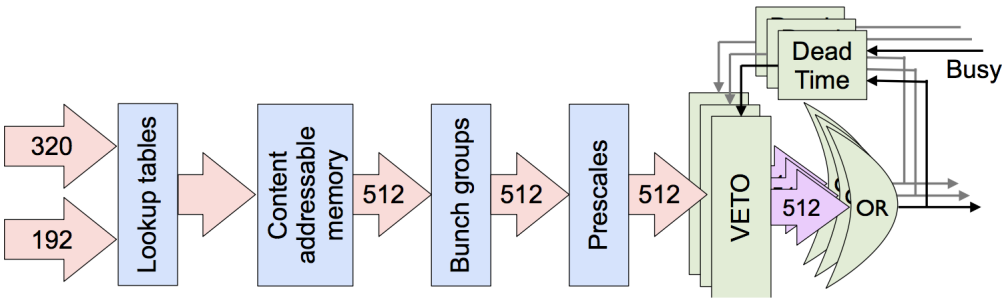

FIGURE 4.7: Schematic view of the first level trigger path. [15]

More precisely looking at figure 4.7, with the information of the calorimeters and the muon detectors the CTP creates in total 512 possible trigger items (320 form the L1 calorimeter system and the L1 muon system, 192 from L1 Topological trigger modules) using logical tables (truth tables). Those tables perform OR operations and a content addressable memory is used to perform AND and NAND operations. An example of a trigger item can be "1EM10" which means that at least one electron/photon candidate above a p_T-threshold of 10 GeV is required to select the event. The trigger menu defines the list of L1 and HLT trigger items. To ensure an optimal trigger menu within the rate constraints, prescale factors can be applied to L1 triggers (as well on the HLT triggers). At the L1, this is used to keep the total L1 rate below 100 kHz. [15]

A step before the prescale factors is the use of bunch groups. This allows the triggers to include specific requirements on the LHC proton bunches colliding in

ATLAS. The bunches in LHC are identified by the Bunch Crossing Identifier. There are also empty ones which are called gaps. A bunch group is a list of BCID's which the trigger is active on. For example one bunch group can be "paired" meaning that the trigger requirements include paired colliding bunch-crossings. There are in total 8 bunch groups which form a Bunch Group Set. All L1 trigger items have one or more explicit or implicit bunch group requirements. They can also carry the bunch group in their trigger chain name like `L1_EM3_EMPTY` where "empty" is one bunch group also. Or for random triggers `L1_RD0_FILLED` where "filled" is a bunch group.

At the end the OR of all trigger items the L1 Accept signal is sent to all sub-detectors to trigger their read-out depending if the the L1 criteria is passed or not.

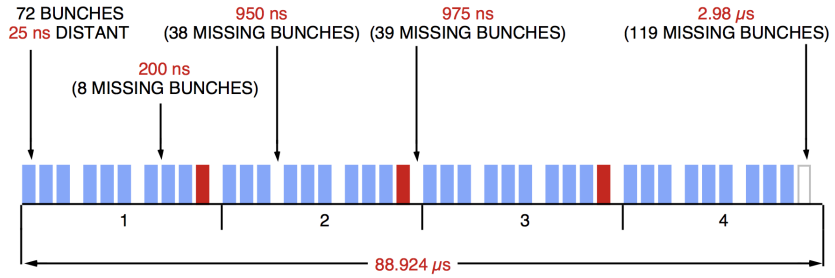

FIGURE 4.8: Revised LHC bunch structure [42]

Important also is the trigger dead-time. The dead-time means the span of time during which the trigger is unable to operate. To handle dead time at the trigger level, meaning that the buffers of the readout electronic becoming full, the CTP generates two types of dead time. One of them is the "simple" dead time which is the number of bunch-crossings that the trigger waits before a new L1 accept. So it is the number of bunch-crossings vetoed after each L1 accept. The other one is the "complex" dead time which is generated by the CTP using a leaky-bucket algorithm. The algorithm can be explain in a simple way [16] : it is a bucket which leaks with a constant rate and is increased by a given value each time a L1 accept occurs. When the bucket is full, dead time is introduced. The parameters of this algorithm determine the maximal number of L1 accepts before dead time is generated. In other words, it restricts the number of L1 accepts in a given period. When dead time is applied, the events are vetoed and cannot be selected for a L1 accept signal.

4.4 The High Level Trigger

The events which are accepted at the Level-1 are then send to the HLT. The HLT is a real-time software system that performs the final online selection of events. The HLT uses finer-granularity calorimeter information, precision measurements from the MS and tracking information from the ID, which are not available at L1. It uses those informations to run algorithms that reconstructs different object of interest or to apply selection cuts. So at a general case, the algorithms can be of two types :

- Feature Extraction (FEX) which are algorithms that creates the objects of interest like tracks or clusters.
- Hypothesis (HYPO) which are the algorithms that apply the selection cuts, for example on the p_T of the tracks.

The Level-1 feeds the HLT with regional information, that is the Regions-of-Interest (RoI's) (figure 4.1). The algorithms can either be done within the RoI's or within the full detector. This stage has two main steps : a fast first-pass reconstruction and a precision reconstruction. The fast pass reconstruction consists to reject the majority of the events which do not pass the selection and then the precision reconstruction which is executed on the remaining events.

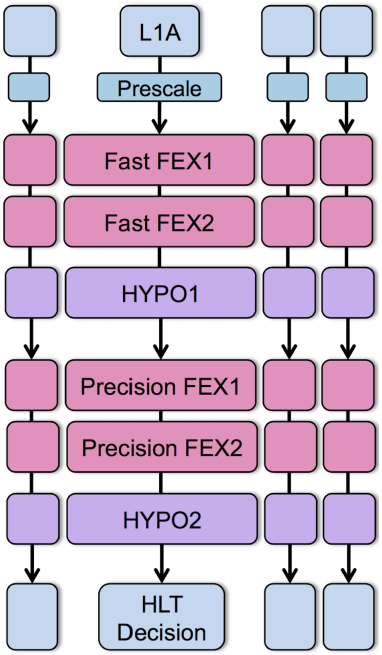

FIGURE 4.9: Scheme of High Level Trigger reconstruction software.[45]

So the trigger at the HLT works in steps as seen in figure 4.9. There are "chains" where each chain looks at a specific selection for a specific signature of interest. First as said before, a fast reconstruction within the RoI's is done. Those fast algorithms within the RoI's build the object of interest like the tracks and the clusters. After this, an HYPO algorithm is done at the RoI's to apply selections on the variables of interest, like on the p_T of the tracks. If the event passes, the two same type of algorithms are executed but at the full detector level, meaning the precession reconstructions. If on of these steps fails, the chain stops the processing.

To be able to process those algorithms the HLT is based on software which runs on commercial computing farms that are installed in the surface building above ATLAS. The processing time is handled by about 28 000 available CPU cores. An important note is that the HLT reconstruction algorithms are very similar to the offline reconstruction algorithms. These would be identically in the ideal case but the offline reconstructions takes to much time compared to the available HLT reconstruction algorithms.

4.4.1 Calorimeter algorithms

As said before, the HLT uses the information of the different sub-detectors of ATLAS. The signals from the calorimeters are used by algorithms (FEX) to convert them into the objects of interest : clusters and cells. Those are then used as input to algorithms which reconstructs of electron, photon, tau, and jet candidates. The HLT algorithms have access to the full detector granularity and so there is an improvement in accuracy and precision in energy and position compared to at L1.

The calorimeter algorithms have different stage depending on which candidates looking at. Before processing with the HLT algorithms, retrieving the data is needed. It concerns either the data from within the RoIs identified at L1 or the data from the full calorimeter. The data from within the RoIs is to reconstruct distinct and localised objects like electrons, photons, muons or taus. On the other hand, the full calorimeter reconstruction is used for jets and more global event quantities. In the both case, the retrieved data is converted into a collection of cells. After the retrieving of data, the cluster algorithms are processed to group these cells and to sum the total deposited energy within each cluster. There are two different clustering algorithms :

- the sliding-window algorithm
- the topo-clustering algorithm

The topological clustering algorithm is used to reconstruct jets, taus and the missing transverse energy. In simple words the idea of the algorithm is to group into clusters neighbouring cells that have significant energies compared to the expected noise. This makes a cluster which has a variable number of cells, in contrast of the sliding window algorithm which has a fixed size window and so a fixed number of cells. The algorithm starts with a seed cell which has a large enough energy significance (signal to noise ratio) compared to a threshold. The neighbouring cells are then added up if their energy significance is above a low threshold. Then one of the neighbouring cells can serve as a seed cell like before and expands the cluster if its significance is above a medium threshold. So there are three thresholds where the low threshold ensures that tails of showers in the calorimeter are not discarded and the higher threshold are used for the seeds and neighbours. Each of those algorithms as said before, are done also offline.

4.4.2 Inner detector tracking algorithms

The inner detector tracking algorithms (FEX) gives the track informations. It can be divided by two stages: a fast tracking and a precisions tracking. The fast tracking algorithm is a trigger which is based on pattern recognition algorithms (not related with the hardware Fast TracKer(FTK)). The precision algorithms is based a lot on the offline tracking algorithms. Those tracking algorithms run during the HLT processing, only at the RoI's identified by the L1 because of processing time. So a full detector tracking informations are not available.On the contrary for the offline tracking algorithms runs in the complete detector, once per event. So tracking information at the full detector is only available for offline if FTK (Fast TracKer) would not be implemented. [37]

4.5 The Fast TracKer

As said before, the full detector tracking information at the trigger level is not easy to implement and before FTK, was not available. It is instead reconstructed only within the RoI's during the HLT processing. But with the new hardware called Fast TracKer (FTK) full-detector tacking information is available. This hardware performs a full detector track reconstruction for tracks that has a $p_T > 1$ GeV. To do so FTK uses the pixel and semiconductor tracker information from the inner detector with the data from Level-1 trigger. Implementing FTK provides a full event track information to the HLT at the L1 rate of 100kHz. The output of FTK is carried to the HLT and so will help the HLT to process the reconstructions of objects, given the full tracking information. The key feature and the core of FTK is based on an idea originated the 1980', what is called the associative memories in parallel. That system stores in FTK millions of pre-calculated patterns and then compare them in parallel with the data coming from the silicon detectors.

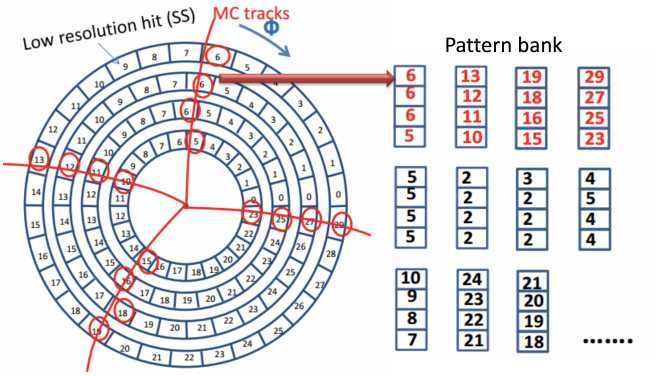

FIGURE 4.10: Pattern banks generated with MC tracks for FTK.[45]

Tracking consists in general of two steps: first the track finding (or pattern recognition) and then the track fitting. The major challenge of tracking is when performing the track finding because of the limited latency of the trigger. The number of hit combinations that have to be tested increases like $\sim L^n$, where L is the instantaneous luminosity and n is the number of silicon layers at the inner detector. This leads to a challenge but the method of the associative memory in parallel allows for a faster track finding which is applicable to the triggers. So the track finding is done based on a on pattern matching. Pattern banks are generated before hand using MC simulations with more than 50 billion tracks used which gives $\sim$ 1 billion patterns (figure 4.10). Then the hits from data are compared to the to existing track patterns and a track fitting is performed (figure 4.11). The reconstructed track information and hit information are then sent to the ATLAS ReadOut System (ROS) and used at the HLT. With this implemented the HLT can reconstruct all the vertices in an event which makes better separation of primary vertex and pile-ups. [44]

4.5.1 Track reconstruction with FTK

The FTK reconstructs tracks using one layer of the Insertable B-Layer, 3 layers of the Pixel detector, and 8 layers of the Semi-Conductor Tracker (Section 2). As said before, FTK operates with two steps. First step is to find track candidates with the the pattern banks and the second step is track fitting. For the track finding 8 layers of the inner detector is used and for the track fitting with the full 12 layers. The algorithms

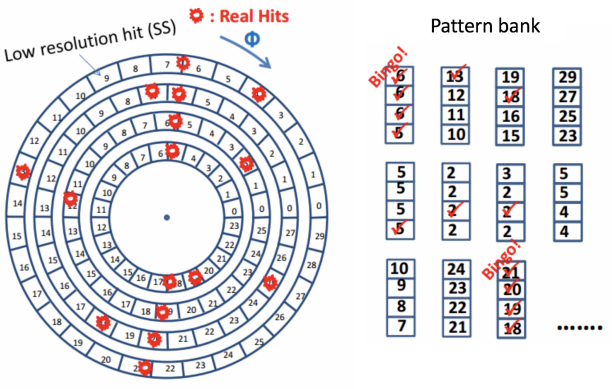

FIGURE 4.11: Pattern banks to perform a track fitting for FTK.[45]

used and the once who are key are the pattern matching algorithm and the linear approximation algorithm. In the case for the pattern matching, as explained before, track candidates are found among pre-calculated track patterns who are made from MC. After that the track candidates are found, the track fitting is used.

The track fitting is done with a linear approximation of local hit positions with full resolution of the inner detector. For the fitting there are 5 track parameters and the χ^2 components are used. The linear approximation is done by scalar products of the hit coordinates and pre-calculated fit constants which takes into account the geometry and alignment of the detector. The 5 track parameters are calculated as follow:

$$p_i = \sum_{l=1}^{N} C_{il} x_l + q_i \tag{4.1}$$

with x_l the hit coordinates of N hits and C_{il}, q_i are pre-calculated constants form the pattern matching with the pattern bank from the MC tracks. So when hit coordinates are given, the calculation of the track parameters and the χ^2 components is done. The fit is performed in each layer and a set of fit constants is defined. [32]

First, the track fitting is performed as said before, by 8 layers of the inner detector. The tracks which pass the χ^2 requirement are passing through the second part of the fitting. We call a recovery fit the case when a track has hit points in all layers but that it fails the χ^2 requirement by not too much, then a refitting is performed a couple of times and each times a hit in a layer is removed. The recovery fit takes into account when a hit is lost due to detector inefficiency and a random hit is picked up instead. The case when there are two tracks which passes the χ^2 requirement on the same road meaning shares a number of same hits, then the best is kept based on the χ^2.

The second part of the fitting is performed when the track passes the first one. In this case then the track fitting is performed using all 12 layers by extrapolating 4 layers which are not used at the first stage. The χ^2 requirement is used like the first step. The tracks which passes this are sent to the Read-Out System (ROS) and used at the HLT. [34] [33] [44]

Chapter 5

Performance studies and multi-jet trigger improvements

This study uses the JVT variable to suppress as much as possible the pile-up from a specific event selection. First the reconstructed offline jets are considered and then the online jets using the information of the offline jets. An important idea in this thesis is the following : because the JVT variable is only available for the reconstructed offline jets (section 3.5) and online JVT is not yet available, a matching between online and offline jets is necessary to benefit of the JVT information. In other words, this study will "emulate" online JVT by matching online jets to offline jets to provide an approximation for online JVT values. Those offline JVT values are then assigned to online jets to further emulate the full trigger selection. Doing so, the performance is studied by checking on the rates and the signal efficiencies.

The efficiency of the trigger selection is an important performance aspect to be studied. Each trigger selection (chain) is associated with an efficiency. It tells how well the trigger performs on the given trigger selection. A new selection can improve the efficiency for no significant increase in rate, or leave the efficiency unaffected for a significant decrease in rate.

Trigger efficiency is an estimation of a selection efficiency. Knowing the selection efficiency is important in high-energy physics, for example when dealing with a trigger or offline event selection with the aim of measuring a cross section. The selection efficiency is the conditional probability for a given condition, that any single event passes the selection. To know the efficiency, one must specify at least selection X (the trigger chain), preselection S (the sample) and if any, reference quantity q (for example a looser trigger selection). So the efficiency $\epsilon_X(q;S)$ is the probability that one event in sample S passes the trigger selection X as function of the value of q. So formally with the conditional probability [23] :

$$\epsilon_X(q;S) = P(X|S,q) \tag{5.1}$$

remembering that $P(A,B) = P(A|B)P(B) = P(B|A)P(A)$.

The simplest case is when the event belongs to the sample S. When q is a simple event counting. The procedure is to count the initial number of events n_S in sample S, count the final number of events k_A after requiring X and then estimate the efficiency with the observed relative frequency :

$$\epsilon_X(S) \approx f_S \equiv \frac{k_A}{n_A} \tag{5.2}$$

From the Bernoulli's theorem, when $n_A \to \infty$, f_S converges in probability, to the true in the beginning unknown, efficiency.

5.1 Pile-up mitigation with tracks

5.1.1 Event selection

Ideally online jets are the same as the reconstructed offline jets but this is not possible due to time limits because of the high rate. The trigger decision needs to be taken fast. So the relevant improvement has to be used at the relevant trigger selections to provide optimal online-to-offline correlation. Therefore, the event selection on the offline jets must be relevant to the trigger decision (trigger menu) that has been used.

In these studies the following event selection has been chosen. Events with at least 6 central jets; central jets are defined as jets with $|\eta| < 2.4$; and each jet has the following conditions :

- in the case of having a lower or equal a p_T of 60 GeV, must pass a certain JVT criterion
- or has at least a p_T of 60 GeV or above.

The selection is done based on the following information. First, is that for jets with a p_T higher than 60 GeV the jet is considered to come from the primary vertex of the hard scatter interaction. The central jets ($|\eta| < 2.4$) who have less than 60 GeV of p_T are to be selected by the JVT criterion.

Goals of the study

The main goal of the study is to improve and to evaluate the impact of pile-up jet suppression with JVT on multi-jet trigger chains in the view of FTK. Therefore, the online jets selected by the trigger (trigger chain) and are matched to the offline jets to use their JVT information. The online jets that do not pass the trigger chain decision are not used for the matching. The trigger chains using in this specific study are:

`HLT_6j25_gsc45_boffperf_split_0eta240_L14J150ETA25`

`HLT_7j25_gsc45_boffperf_split_0eta240_L14J150ETA25`

As seen in the trigger chains, only final calibrated jets of at least 45 GeV of p_T are selected. Also the jets are selected to be central meaning that the selection on the η variable is in the range of $[-2.4, 2.4]$. At the Level 1 Trigger this chain takes events with at least 4 jets with at least 15 GeV of p_T each. A lower number of jets requirement or multiplicity at L1 is used in comparison to the HLT. This is simply because if the multiplicity of the L1 would be higher than the HLT, then the HLT selection would not be interesting. In this case, the events with jets that passes the L1 selection would lead necessarily to events with jets that passes the lower multiplicity of the HLT, so at the end no real selection at the HLT would be done and the rate would not change.

For the JVT estimation, offline reconstructed jets via topological clustering and particle flow offline reconstructed jets are used. Evaluation of the impact on the rate

reduction and the signal efficiencies is done. Checking the signal efficiencies using particle flow jets is done which motivates to ensure that HLT can run particle flow in Run3. The data sample which had all the information necessary that is used is :

`data17_13TeV.00339535-00339590.physics_Main.merge.AOD.f889_m1902.root`

This data set is from data of 2017 and is a ntuple which is a TTree from the Tree library of Root. The ntuple has the offline and the online information necessary as well as the information if each event has passed the triggers of interest. The transverse momentum and the two space coordinates η and ϕ are all for the offline and the online jets present as information in the ntuple. Also, for the offline jets the accessible JVT variable is also present.

Matching between offline and online jets

A good correlation between online and offline jets is necessary. If the correlation or matching is not good enough then the information of the offline jets can be too much fluctuating for the online jets. For example in a extreme case, if the correlation isn't good, the leading p_T of the offline jets might not be the leading p_T of the online jets. So a good correlation gives a good certainty of the information between them.

The coordinate system (η,ϕ) of the detector is used. The principle is to take the minimum distance ΔR (section 2.2.1) of the possible matching between the online jets and the offline reconstructed jets and if this minimum ΔR is less than a criterion fixed it is considered a match. The ΔR of the jets from the sample is seen at figure 5.1. The six histograms represents the first, second and so on leading in p_T online jets. Firstly, it can be concluded that as the momentum decreases the more online jets with a higher minimum delta R of around 0.4, appear. Online jets with a minimum distance of 0.4 or less to offline jets is the most dominate for all the p_T online jets. So a $\Delta R < 0.4$ is set to be a good criterion to have a stable count of jets that are matched for the topological clustering reconstructed jets as well as for the particle flow reconstructed jets.

If the minimum distance ΔR of the possible matchings between the online jets and the offline reconstructed jets is less than 0.4, it is considered a match. In other words, if a online jet finds the closest offline jet to be within $\Delta R < 0.4$ it is a match between the two. Looking also at the first six leading online jets, the criterion of $\Delta R < 0.4$ is also considered good for the matching condition (Figure 5.2 and Figure 5.3).

To have an idea of the correlation between the online and offline jets is to look at the difference of p_T when they are matched. The figure 5.4 describes this and tells that the majority of the matched jets have a p_T close to each other.

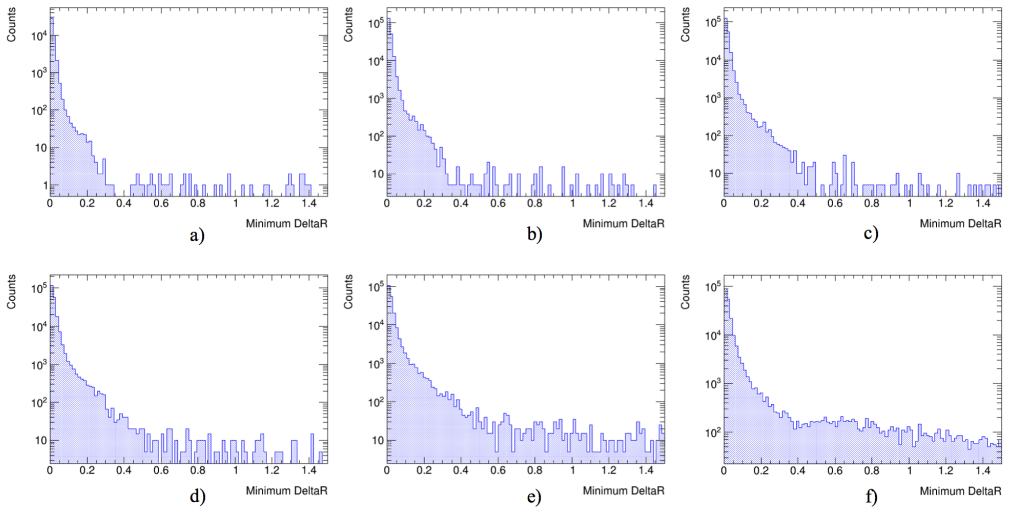

FIGURE 5.1: a) The minimum ΔR values for the first leading online central jets with the topological clustering reconstructed central jets. b), c) d) e), f) respectively the minimum ΔR values for the second, third, fourth, fifth and sixth leading online jets.

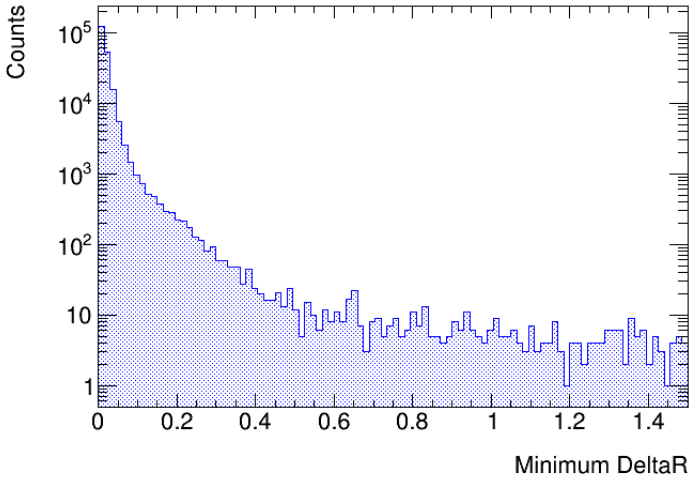

FIGURE 5.2: The minimum ΔR values for the first six leading central online jets with the topological clustering reconstructed central jets.

5.1.2 Impact on rates

The rate reduction in our study is defined as the fraction of events that has been reduced by the addition of the JVT information. The triggered events which are chosen by the trigger chains, can be reduced even more with the JVT. With the event selection (section 5.1.1), the goal is to see how many events has been neglected and so suppress as much as possible JVT considered pile-up for the triggered events.

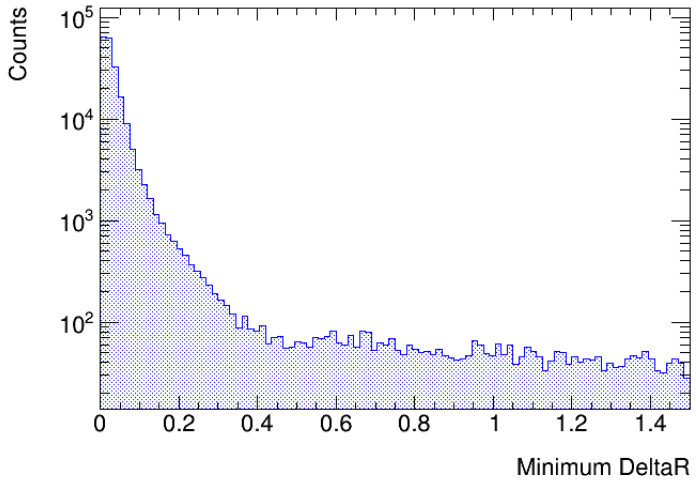

FIGURE 5.3: The minimum ΔR values for the first six leading central online jets with the particle flow reconstructed central jets.

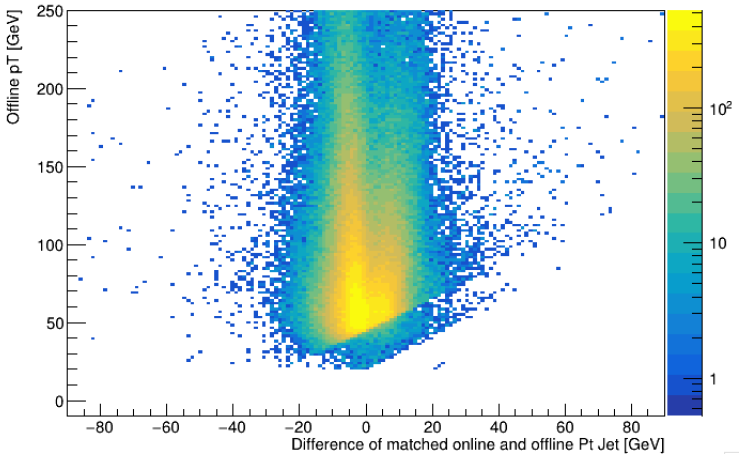

FIGURE 5.4: Offline p_T as a function of the difference in p_T of the matched online and offline jets.

First, the reconstructed jets will be used to see how the JVT can affect for the event selections. This is important for the offline storage usages. If the reduction is good enough then for the same physics, the storage usage decreases. In other words, keeping only the interesting events for the same physics with less storage space used. As a side note, it can also be looked at it in the other way : if for the same rate more physics is demanded, then a less strict selections are used for example a certain p_T threshold. For the triggered online jets, the selections can also be done by using the matched offline JVT information.

Rate for the reconstructed offline jets

The rate reduction for the offline jets can be found with the following ratio R.

$$R = \frac{Nevents\ passed\ JVT\ central\ jets}{Nevents\ total\ central\ jets} \tag{5.3}$$

with the numerator and denominator explained as follow:

- *Nevents passed JVT central jets* : number of events having at least n central jets (with $p_T \geq 45$ GeV) where each jet has either :
  - a $p_T \geq 60$ GeV
  - or passing the JVT criterion when the p_T is between 45 GeV and 60 GeV.
- *Nevents total central jets* : number of events having at least n central jets where each jet has a $p_T \geq 45$ GeV.

With $n = 6$ or $n = 7$ depending on the trigger chain used for the online jets afterwards in this chapter. The p_T cut value, on whether or not the JVT criterion is used is set to be here at 60 GeV. This can be changed as will be discussed later. The JVT criterion will be a value between 0 or 1 as explained before. The events used in this studies are coming from data samples and so contain mostly background. Using this same fraction looking only at the signal of interest gives the efficiency.

Table 5.1 is a table with the rates for topological clustering jets with $n = 6$. The values are for different JVT cut values but with the same cut on the p_T value of 60 GeV (*Nevents passed JVT central jets*).

JVT cut value	Fraction of events after pile-up suppression	Fraction of jets passing selection per event
0.1	76.22%	93.85%
0.2	73.57%	93.05%
0.3	72.63%	92.76%
0.4	71.45%	92.42%
0.5	70.83%	92.21%
0.6	70.01%	91.98%
0.7	69.17%	91.74%
0.8	67.98%	91.39%
0.85	67.01%	91.13%
0.9	65.73%	90.75%

TABLE 5.1: Table of the rates for $n = 6$, topological clustering reconstructed jets with looser JVT cuts but with a fixed p_T cut value of 60 GeV

The third column of the table gives the fraction of jets passing the selection per event. This number is not the most important one but can give an idea of how many jets per events are selected. This percentage is pretty high and confirms that per event there are enough jets available for the selection. And about 7% or more are likely coming from pile-up interactions.

The other column gives the percentage of how many events of the total are selected with the pile-up suppression. About 75% to 65% of events are passing the

selection and therefore about 25% to 35% could be removed using JVT. This is equivalent to a rate reduction of 25% to 35%. Loosening the JVT cut as seen in the table 5.1, provides an information on the fact that for example a cut on 0.4 or 0.6 do not change a lot the rates. So a JVT cut of 0.4 compared to the one used usually of 0.59, is good enough for the rate reduction. This could also be potentially the case for the online jets.

The JVT distribution (figure 5.5) confirms the fact that a cut with 0.4 or 0.6 do not change significantly the amount of jets that are selected. This plot also confirms what have been said for the JVT, that the values are between 0 and 1 with -1 which is the value for jets with no associated tracks.

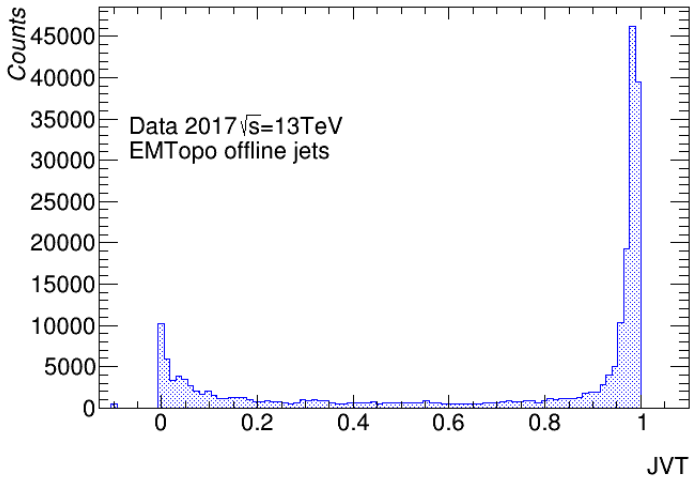

FIGURE 5.5: JVT distribution for the offline reconstructed jets with topological clustering, with the selection of $n = 6$ with $p_T \geq 45$ GeV

Some looser cuts on the p_T can be seen in the table 5.2, nothing unexpected happens. The JVT cut is fixed at the value of 0.59 (which is the one most commonly used). The higher the p_T cut is the less events are selected, the more the rate reduction goes up.

p_T cut value [GeV]	Fraction of events after pile-up suppression	Fraction of jets passing selection per event
60	70.12%	92.01%
65	66.75%	90.56%
70	64.77%	89.55%
75	63.26%	88.76%
80	62.33%	88.15%
85	61.52%	87.57%
90	60.96%	87.29%

TABLE 5.2: Table of the rates for $n = 6$, topological clustering reconstructed jets with looser p_T cuts but with fixed JVT cut value of 0.59

Looking also at a looser p_T cut for a fixed JVT value of 0.4, proves that the rates are almost identical (table 5.3).

p_T cut value [GeV]	Fraction of events after pile-up suppression	Fraction of jets passing selection per event
60	71.45%	92.42%
65	68.23%	91.05%
70	66.33%	90.09%
75	64.90%	89.34%
80	64.05%	88.78%
85	63.33%	88.33%
90	62.85%	87.99%

TABLE 5.3: Table of the rates for $n = 6$, topological clustering reconstructed jets with looser p_T cuts but with fixed JVT cut value of 0.4

The same can be done for $n = 7$, meaning selecting at least 7 jets with $p_T \geq 45$ GeV. The same conclusion as for $n = 6$ can be said. But with a slightly higher fraction of events that are selected with the pile-up suppression (tables 5.4 and 5.5).

JVT cut value	Fraction of events after pile-up suppression	Fraction of jets passing selection per event
0.1	75.92%	94.44%
0.2	73.24%	93.72%
0.3	72.49%	93.45%
0.4	71.62%	93.14%
0.5	70.67%	92.90%
0.6	70.31%	92.77%
0.7	69.52%	92.56%
0.8	68.22%	92.24%
0.9	66.44%	91.71%

TABLE 5.4: Table of the rates for $n = 7$, topological clustering reconstructed jets with looser JVT cuts but with a fixed p_T cut value of 60 GeV

p_T cut value [GeV]	Fraction of events after pile-up suppression	Fraction of jets passing selection per event
60	70.31%	92.79%
65	66.79%	91.48%
70	64.82%	90.58%
75	63.35%	89.73%
80	62.33%	89.12%
85	61.62%	88.59%
90	61.06%	88.23%

TABLE 5.5: Table of the rates for $n = 7$, topological clustering reconstructed jets with looser p_T cuts but with fixed JVT cut value of 0.59

If now the p_T cut is neglected, then the JVT cut is applied on all the jets with $p_T \geq 45$ GeV and not only on jets with a p_T between 45 GeV and 60 GeV. The expectation is that the rate reduction increases because the pile-up suppression is applied on all the jets of our selection (table 5.6).

JVT cut value	Fraction of events after pile-up suppression	Fraction of jets passing selection per event
0.1	67%	89.06%
0.2	63.84%	87.65%
0.3	62.49%	87.08%
0.4	61.01%	86.50%
0.5	59.92%	86.08%
0.59	58.80%	85.67%
0.6	58.73%	85.62%
0.7	57.47%	85.16%
0.8	55.26%	84.40%
0.9	51.33%	83.06%

TABLE 5.6: Table of the rates for $n = 6$, topological clustering reconstructed jets with no p_T cuts, all the jets

Rate for the matched online jets

The rate for the online jets is of great interest. First, the online jets as mentioned before, have to be matched to the reconstructed jets. This is necessary to apply the JVT cut on them and so to be able to suppress the pile-up. Depending on the correlation of the online and offline jets it can fluctuate but from the previous study on the correlation this can be done properly.

The rate reduction for the online jets matched to the offline jets (passing the criterion $\Delta R < 0.4$) can be done using the following ratio $R_{matched}$:

$$R_{matched} = \frac{Nevents\ passed\ JVT\ central\ jets\ matched}{Nevents\ total\ central\ jets\ matched} \tag{5.4}$$

- *Nevents passed JVT central jets matched* : number of events having at least n central online matched (passing the criterion $\Delta R < 0.4$) jets (with $p_T \geq 45$ GeV) passing the trigger selection of interest where each jet has either:
  - a $p_T \geq 60$ GeV
  - or passing the offline-matched JVT criterion when the p_T is between 45 GeV and 60 GeV.
- *Nevents total central jets matched* : number of events having at least n central online matched jets with $p_T \geq 45$ GeV (*the total central jets*) passing the trigger selection of interest.

The trigger chain used to do the online selection is the following :
`HLT_6j25_gsc45_boffperf_split_0eta240_L14J150ETA25`.
So $n = 6$ and the JVT will be a value between 0 or 1 as explained before. And as before, the p_T cut value which decides on whether or not the JVT criterion is used, is set to be here at 60 GeV. This can be changed as will be discussed later.

Rate for the online jets matched with topological cluster reconstructed jets

First the matching with the reconstructed jets from the topological clustering is considered. As can been seen at figure 5.2, the number of jets under a minimal distance

JVT cut value	Fraction of events after pile-up suppression	Fraction of jets passing selection per event
0.1	71.44%	92.58%
0.2	68.21%	91.51%
0.3	66.85%	91.08%
0.4	65.45%	90.63%
0.5	64.52%	90.31%
0.6	63.58%	90.01%
0.7	62.52%	89.68%
0.8	61.13%	89.25%
0.85	60.11%	88.93%
0.9	58.65%	88.47%

TABLE 5.7: Table of the rates for $n = 6$, online jets matched to the topological clustering reconstructed jets with looser JVT cuts but with a fixed p_T cut value of 60 GeV

ΔR is high enough. The offline-matched JVT information can be used, and can be set at different cuts (table 5.7).

The values of the second column confirms that the pile-up suppression using the JVT is performing well. The fractions of events left after pile-up suppression are between 70% and 60%. This gives a equivalent rate reduction of 30-40%. Also, still a good rate reduction for a looser JVT cut can also be concluded. So different JVT cuts are possible and are useful to maintain a good efficiency.

As for the offline jets, a different p_T cut can be chosen (table 5.8).

p_T cut value [GeV]	Fraction of events after pile-up suppression	Fraction of jets passing selection per event
60	63.70%	90.05%
65	60.62%	88.56%
70	58.52%	87.43%
75	57.27%	86.58%
80	56.31%	85.93%
85	55.6%	85.42%
90	55.06%	85.03%

TABLE 5.8: Table of the rates for $n = 6$, online jets matched to the topological clustering reconstructed jets with looser p_T cuts but with fixed JVT cut value of 0.59

The same as for the offline jets, the higher the p_T cut the less fraction of events passes the selection. And also a rate reduction of 36.3% for a JVT cut at 0.59 is still good.

Rate for the online jets matched with particle flow reconstructed jets

Matching with the particle flow reconstructed jets gives us the following results (tables 5.9 and 5.10).

The same trend is followed, when applying different JVT cuts the fraction of events after pile-up suppression do not change by a lot. The rate reduction is still

JVT cut value	Fraction of events after pile-up suppression	Fraction of jets passing selection per event
0.1	77.62%	94.54%
0.2	74.61%	93.61%
0.3	73.22%	93.20%
0.4	71.98%	92.83%
0.5	70.93%	92.52%
0.6	69.86%	92.22%
0.7	68.83%	91.93%
0.8	61.13%	91.52%
0.85	66.29%	91.19%
0.9	64.90%	90.77%

TABLE 5.9: Table of the rates for $n = 6$, online jets matched to the particle flow reconstructed jets with looser JVT cuts but with a fixed p_T cut value of 60 GeV

p_T cut value [GeV]	Fraction of events after pile-up suppression	Fraction of jets passing selection per event
60	69.92%	92.24%
65	66.85%	90.98%
70	64.74%	90.01%
75	63.45%	89.28%
80	62.47%	88.71%
85	61.69%	88.25%
90	61.06%	87.90%

TABLE 5.10: Table of the rates for $n = 6$, online jets matched to the topological clustering reconstructed jets with looser p_T cuts but with fixed JVT cut value of 0.59

good for a JVT cut at 0.2 or 0.3. Nevertheless, the rate reduction is smaller in comparison to the online jets matched to the topological clustering reconstructed jets. This is because the intrinsic particle flow pile-up suppression is not taken into account. This means that the already suppressed pile-up from the reconstructed and then calibrated particle flow jets are not taken into account, which will be discussed later.

The dependence of the rate reduction on the number of reconstructed primary vertices N_{PV} is shown at figure 5.3. The N_{PV} can be divided into three parts (figure 5.6). The same selection is done with a JVT cut of 0.59 but considering different N_{PV} intervals.

It can be seen on table 5.11 that the rate reduction changes for different N_{PV} intervals and especially increases 5% for events with N_{PV} >62.5.

To look at the intrinsic particle flow pile-up suppression no JVT cut is used and the ratio is defined as the number of events having at least 6 central online matched jets passing the trigger divided by the total number of events having at least 6 central online jets (not matched). It can be written as $\frac{matched}{notmatched}$. It translates the effect of the online jets who are matched to the particle flow jets, so the intrinsic particle

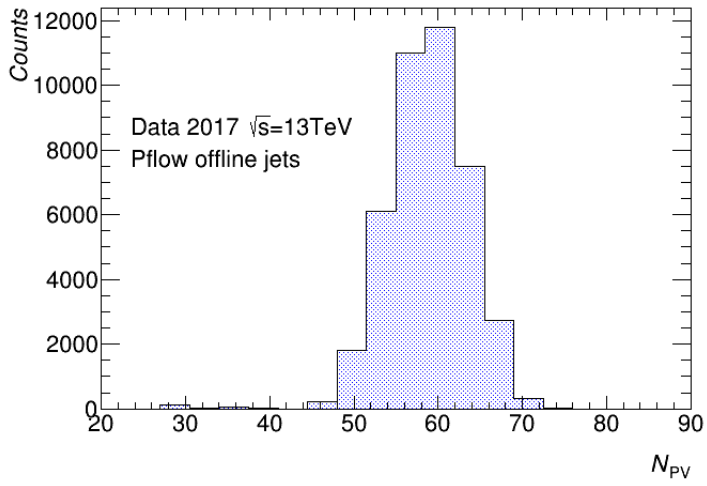

FIGURE 5.6: Number of reconstructed primary vertices (N_{PV}) from particle flow reconstructed jets.

	Fraction of events after pile-up suppression	Fraction of jets passing selection per event
$\forall$ values of N_{PV}	69.92%	92.24%
$N_{PV} < 55$	73.51%	93.35%
$N_{PV} \in [55, 62.5]$	70.64%	92.44%
$N_{PV} > 62.5$	64.58%	90.65%

TABLE 5.11: Table of the rates for $n = 6$, online jets matched to the particle flow reconstructed jets with N_{PV} dependence with JVT value fixed at 0.59 and p_T cut at 60 GeV

	Fraction of events after pile-up suppression
$\forall$ values of N_{PV}	88.36%
$N_{PV} < 55$	89.62%
$N_{PV} \in [55, 62.5]$	88.60%
$N_{PV} > 62.5$	86.59%

TABLE 5.12: Table of the rates for $n = 6$, intrinsic particle flow pile-up suppression

flow pile-up suppression. Looking at the table 5.12, the rates of this intrinsic pile-up suppression is about 10% and gives no big changes for different N_{PV} intervals.

The effect of the JVT only on the rate can also be shown (Table 5.13). For this another ratio is defined : the number of events having at least 6 central online matched jets (with $p_T \geq 45$ GeV) passing the trigger and with the JVT cut divided by the total number of events having at least 6 central online jets (not matched). It can be written as $\frac{matched+JVT}{notmatched}$.

A conclusion can be made for this part of the study. There is about 30% to 40% of rate reduction when JVT is considered using either topological clustering reconstructed jet and particle flow reconstructed jets for the matching. Ans also that there

	Fraction of events after pile-up suppression
$\forall$ values of N_{PV}	61.79%
$N_{PV} < 55$	65.88%
$N_{PV} \in [55, 62.5]$	62.58%
$N_{PV} > 62.5$	55.92%

TABLE 5.13: Table of the rates for $n = 6$, effect of JVT cut

is an more important impact on the rate (about 5%) for (about 10%) higher pile-up.

5.1.3 Impact on efficiency

In this study, the efficiency is used in the analysis to look at the online jets corrected with the matched-to-offline JVT cut and selected with the trigger selection (chain) used. The trigger chain used for the online jets is :

`HLT_6j25_gsc45_boffperf_split_0eta240_L14J150ETA25`

As explained in the beginning of the chapter, to provide the best correlation between the online and offline jets, the offline reconstructed jets are selected at the relevant trigger selections used for the online jets. Looking at the online jets triggered with the chain mentioned above, a reasonable event selection for the sample S is 6 offline reconstructed jets with each one of them checked for JVT cut. The selection X on the sample S is 6 online jets with the matched-to-offline JVT cut selection as this is to suppress the pile-up. It can be written as follow :

$$efficiency(p_T) = \epsilon(p_T) = \frac{\sum_n (\textit{event sample } S \;\&\&\; \textit{trigger selection } X | p_T)}{\sum_n (\textit{event sample } S | p_T)} \tag{5.5}$$

With the summation over all the events n and with the following correspondances:

- *event sample S* : 6 offline reconstructed jets which are checked for JVT meaning that if p_T< 60 GeV apply JVT cut for $|\eta| < 2.4$, if $p_T > 60$ GeV pass.
- *trigger selection X* : on the events found in sample S an extra selection (selection X) corresponding to 6 online jets with the matched-to-offline JVT selection.

If the selection X is very efficient then all events will be picked from sample S and so efficiency will be close to 1. But on the contrary if the efficiency is not good then no events will be taken into account and the efficiency will be close to 0. In general, the main points to look at for efficiency curves are the following :

- Where does the trigger turn on ? Meaning at which value on the x axis does the trigger efficiency plateaus. Or in other words, at which value the trigger does his expected job of selecting efficiently the right events.
- What is the plateau efficiency ? Does the trigger reach 100% efficiency ? And if so, does the plateau stay flat, meaning is it constant for higher values on the x axis ?
- Does it has enough statistics ? Meaning do enough events passes the trigger selection such that the efficiency curve can be analysed.

The steepness of the slope of the efficiency curve and the peak efficiency varies and in an "ideal world" would resemble to a step-function (Figure 5.6). The variation can be explained by the fact that the turn-on and the peak are in function of the resolutions, inefficiencies and the online to offline differences. As said before, the online and offline correlation is an important aspect and can make that the efficiency varies. The main point is that the slope of the efficiency curve has to be the most steepest possible because the trigger has to select the events in the most optimal possible way. As seen in the definition, the efficiency curve is always defined with respect of the objects reconstructed offline. In the efficiency curves the x axis will be the p_T of the leading offline jet. Every bin will be the efficiency of the p_T bin of the leading offline reconstructed jet. It gives the probability for a fully reconstructed and identified offline object to pass the online trigger requirements.

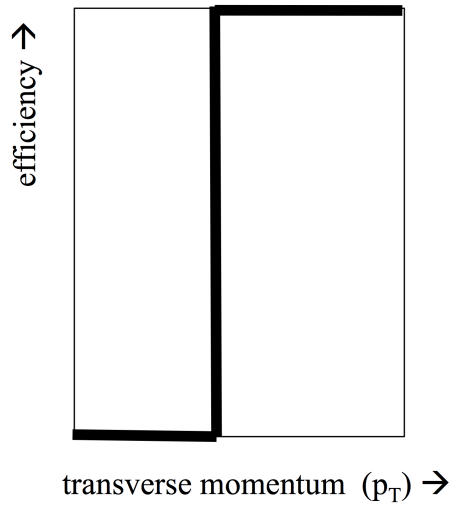

FIGURE 5.7: Trigger efficiency curve in ideal world

Now for the study, the online jets matched to the particle flow reconstructed jets are presented. First, investigating the efficiency curve when using the JVT cut or not for the particle flow reconstructed jets is analysed (figure 5.8).

At the first look, the JVT contribution is clearly important. The slope is steeper in general for the matching with particle flow jets and JVT cut. The turn on for this trigger must be at a p_T value of 45 GeV. On this particular turn-on value the trigger efficiency is approximatively about 80% for both curves (or 0.8 per event efficiency). This means that for a transverse momentum of 45 GeV of the reconstructed jets, about 80% of the events passes the trigger selection of this particular trigger chain. As said before because the online HLT jets are not perfectly the same as the reconstructed offline jets the curve doesn't follow a step-function and do not reach 100% efficiency on the turn-on point. But when the full efficiency is reached, it then stays almost for all the higher p_T values. More precisely, it reaches a plateau of 100% efficiency from 60 GeV on to higher values of p_T. The plateau is flat and provides a stable full efficiency. Since the curves are made from a division of two histograms, the errors are calculated as the square root of the number of entries per bin. So it can be seen that the number of entries which is the number of events, are sufficiently high since the error bars are not large.
Looking at both curves, the use of a JVT cut of 0.59 improves the steepness of the

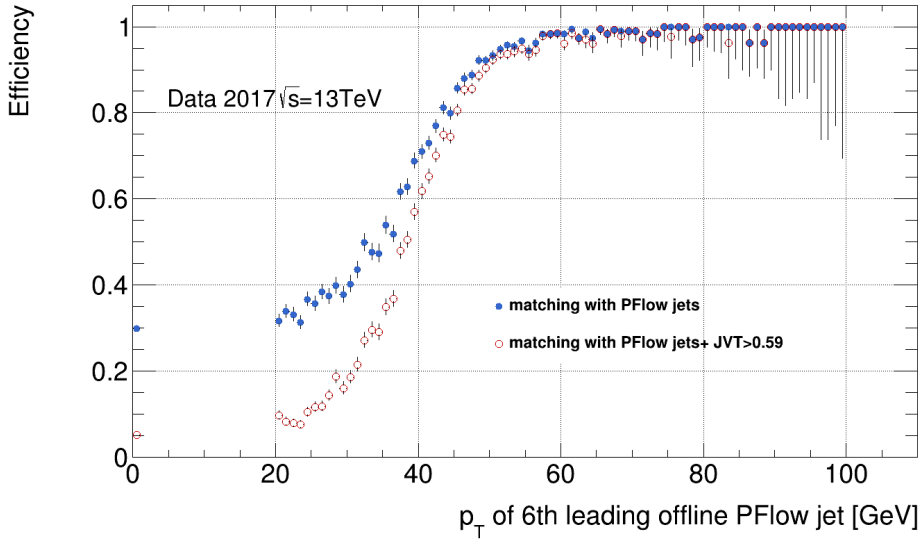

FIGURE 5.8: Efficiency curve for the online jets matched to offline particle flow jets with the trigger chain `HLT_6j25_gsc45_boffperf_split_0eta240_L14J150ETA25`

slope and reduces the number of events that should not have been taken into account in comparison of the curve without the JVT cut. So the JVT cut removes the events which should not have passed by the trigger, and probably is the evidence of JVT working well as a pile-up suppression.

On a side note, to make those curves a division of two histograms was necessary (see efficiency definition eq. 5.5) and therefore the use $TH1 :: Sumw2$ was applied in the code. This method causes the squares of weights to be stored inside the histogram (equivalent to the number of entries per bin if weights of 1 are used). This information is needed to correctly calculate the errors of each bin entry when the method $TH1 :: Divide$ is applied.

From the rate reduction study of the intrinsic particle flow pile-up suppression different efficiencies with different N_{PV} intervals can be shown (figure 5.9).

Looking at the efficiency curves with the different N_{PV} intervals : no changes can be found, they follow all the same trend. The curves have approximatively the same turn on p_T value and the full efficiency plateau stays the same. The curves have the same shape as the red curve of figure 5.8, which is has the same selection but for all N_{PV} intervals. Varying the number of primary vertices there is no significant impact on the efficiency curves.

The plan for Run3 is using the particle flow reconstructed jets instead of the topological clustering jets. With looser JVT cuts it can be seen (figure 5.10) that there is no significantly impact on the reconstructed jets used. Using the particle flow jets with other JVT cuts than 0.59 is good enough compared to the topological clustering jets. The turn-on point stays the same and the full efficiency plateau is stable.

With this a conclusion can be made on a global performance study using the trigger chains `HLT_6j25_gsc45_boffperf_split_0eta240_L14J150ETA25` and

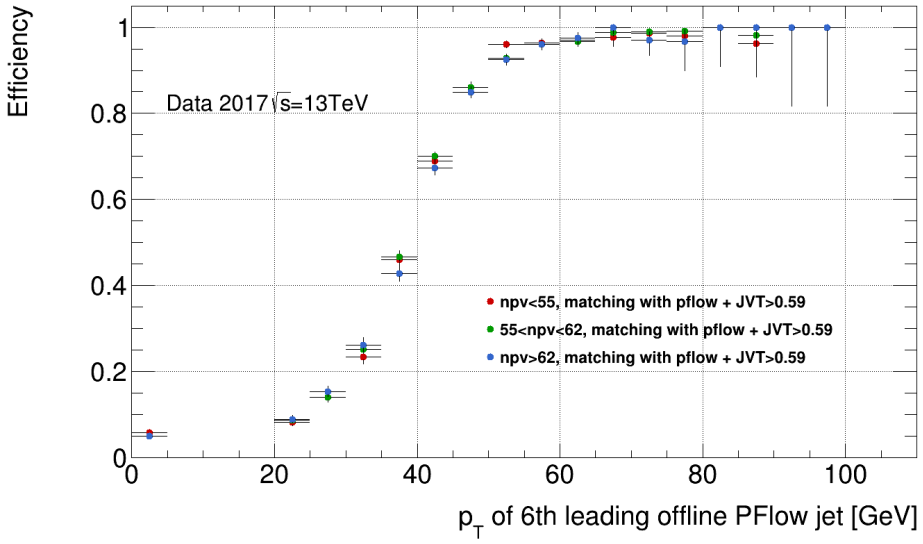

FIGURE 5.9: Efficiency curves with online jets matched to offline particle flow jets with the trigger chain `HLT_6j25_gsc45_boffperf_split_0eta240_L14J150ETA25`

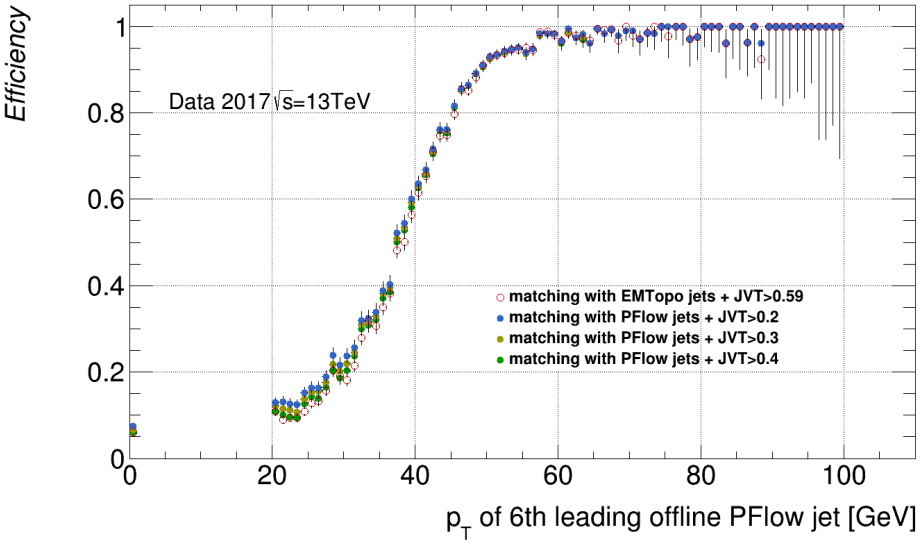

FIGURE 5.10: Efficiency curves with online jets matched to offline particle flow jets and topological clustering offline jets with the trigger chain `HLT_6j25_gsc45_boffperf_split_0eta240_L14J150ETA25`

`HLT_7j25_gsc45_boffperf_split_0eta240_L14J150ETA25`. Looking at the rate reductions, there can be a rate reduction of about 30 to 40 % using the JVT variable to suppress the pile-up. And using particle flow jets there can be a possible another 10% rate reduction looking intrinsically. When applying different pile-up suppressions (looser JVT cut) there is no significant impact on the rate reduction as for the efficiencies. Using the particle flow reconstructed jets as for the matching, a further rate reduction can be seen from 30% to 35% when applying to events with N_{PV} >62. With those rate reduction and with stable efficiency curves information from the

tracks associated to each jet (JVT variable) can be useful in terms of the trigger.

5.2 Performance studies of Run2 data

As a continuation some other triggers from Run2 can be investigated. Various methods can be used to measure other efficiency curves on data. One of the methods to make a turn-on in data, one needs to:

1. Obtain an unbiased p_T spectrum in the range of interest for the efficiency
2. Of these events in the right p_T range, see which pass the trigger of interest

So there is a need of an unbiased p_T spectrum and for that a reference trigger is applied. Looking at all the data, every event by definitions had to pass some trigger. So all the events of the data passed all different kinds of triggers. This is quit a poor analyse because some events are then biased by some triggers. So what is needed is a selection of events free of trigger bias meaning taking a reference trigger which turn-on is known and only consider events on the full efficiency plateau of this trigger in the determination of the probe trigger efficiency. This is not done in the previous study, because only the performance of the JVT pile-up suppression is studied and since all the efficiency curves are made the same way this do not affect the conclusions made.

As an example, looking at the trigger `HLT_7j25_gsc45_boffperf_split_0eta240_L14J150ETA25` the reference chosen is `L1_4J15`. The reference trigger is a looser one with a p_T spectrum range interesting for the probe trigger (Figure 5.11).

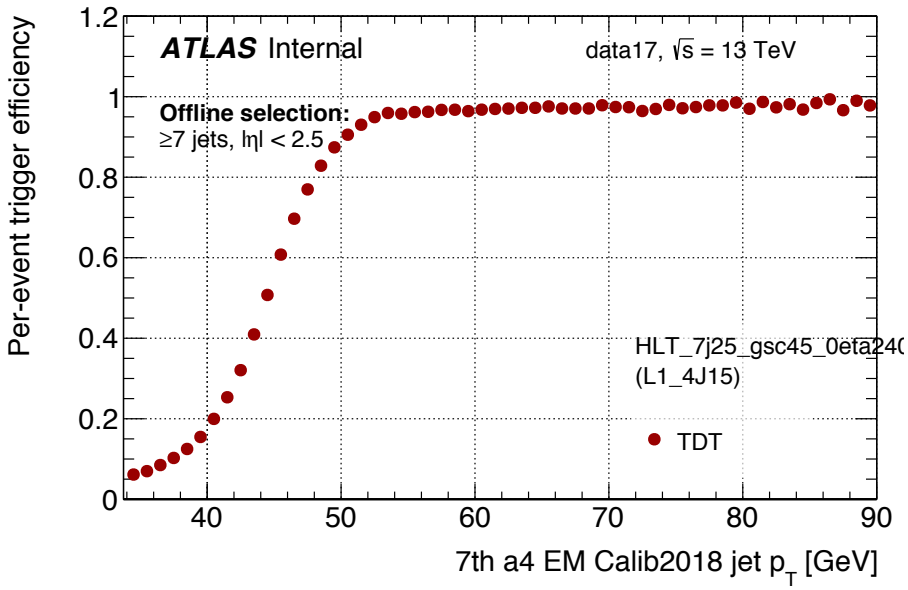

FIGURE 5.11: Efficiency curves with topological clustering offline jets with the trigger chain `HLT_7j25_gsc45_boffperf_split_0eta240_L14J150ETA25` and as reference the trigger chain `L1_4J15`

The efficiency curve of this trigger reaches his plateau around a p_T of 52 GeV of the topological clustering jets. The plateau stays flat without reaching a full 100% efficiency. At the turn-on of the trigger, the efficiency reaches about 50% efficiency.

Level-1 trigger efficiencies

Some L1 triggers can be looked at. Because of the resolution at the L1 trigger is less good than at the HLT, the multiplicity must be smaller at the L1 compared to the HLT. If this is not the case, an inefficiency appear caused by the granularity of the L1 trigger. For example, what appears to be one jet at L1 may correspond to two close-by offline jets; this may result in the L1 trigger not firing and the event being missed which gives a so called close-by inefficiency. This is the case of the trigger `L1_5J15.0ETA25` with as reference `HLT_j45`, seen at figure 5.12 and figure 5.13.

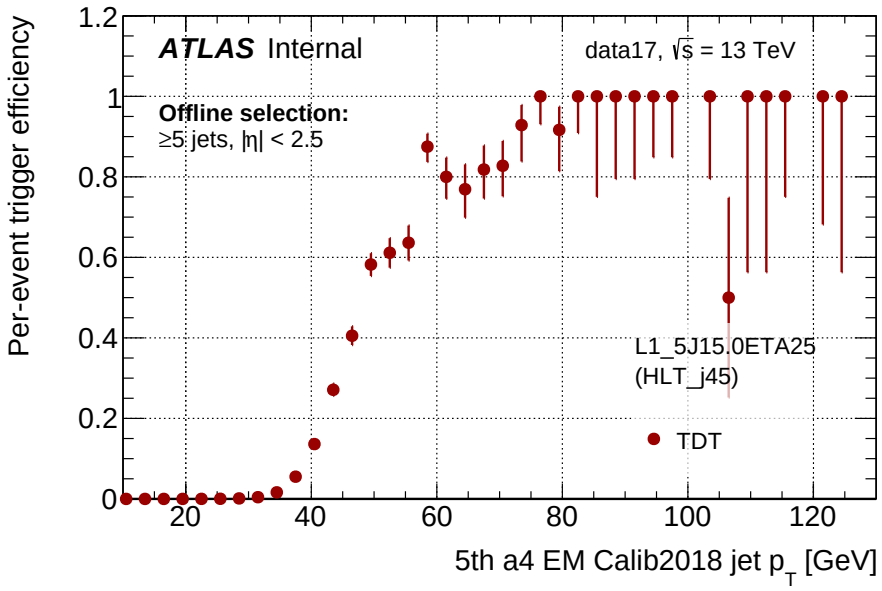

FIGURE 5.12: Efficiency curves with topological clustering offline jets with the trigger chain `L1_5J15.0ETA25` and as reference the trigger chain `HLT_j45`

The efficiency curves of the trigger `L1_5J15.0ETA25` is made with the topological clustering offline jets and the particle flow offline jets. It can be seen that the plateau with the topological clustering offline jets is less flat compared to the one with the particle flow offline jets. A close-by inefficiency is present for the one with the topological clustering offline jets and this can be explained by the fact of the granularity of the L1 trigger as explained earlier.

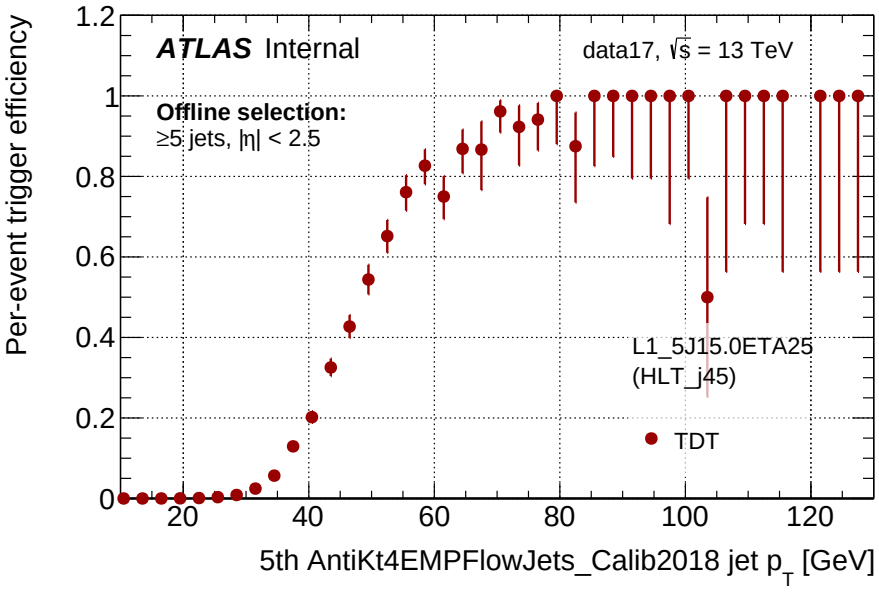

FIGURE 5.13: Efficiency curves with particle flow offline jets with the trigger chain `L1_5J15.0ETA25` and as reference the trigger chain `HLT_j45`

Efficiency curves with real data need to have enough statistics. This all depends on the rates that the triggers has, which is set by the trigger menu. Looking at L1 triggers such as `L1_5J15.0ETA25` the rate is very low.

When there is a collision between opposing proton bunches about 10^9 proton-proton collision happens and the two-level trigger system reduces from 40 MHz to about 1000 Hz the rate. This rate of 1 kHz contains then all the different signatures for the physics of interest. Each signature determined by the triggers, like 4 jet events, 6 jet events, 2 muons, etc. Each signature has his own rate set by the trigger menu and summing up to the total output of about 1 kHz. The rate is controlled by selection requirements or prescales. Firstly an unprescaled trigger means that a p_T cut is applied and that events with jets above that certain p_T cut are taken into account, it is the selection requirement that controls the rate in this case. Secondly, an option is to set a prescale factor N. This means that of the total events only 1 of N is taken at random. This lowers the event count by a lot but lowers also the rate.

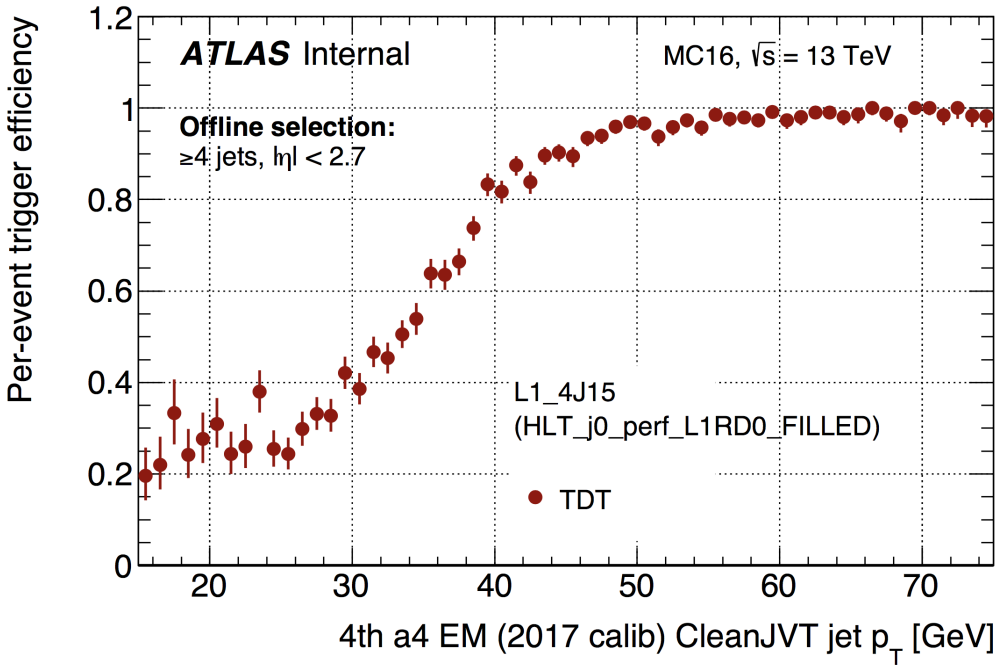

FIGURE 5.14: MC efficiency curves with topological clustering offline jets with the trigger chain `L1_4J15` and as reference the trigger chain `HLT_0j_perf_L1RD0_FILLED`

This leads to the usefulness of MC set of data. When chosen properly, this can give enough events for the chosen signature. The particularity and difference with real data is that MC is generated for a specific signature and not like real data which has all different kinds of signatures. For example to look at some multi-jet triggers, a MC generated with the decay of $t\bar{t}$ is used. The top quark pair production in the fully hadronic final state is characterised by a six jet topology which is very useful for multi-jet triggers (figure 5.14).

Chapter 6

Conclusion

In conclusion, this thesis summarises performance studies and multi-jet trigger improvements in the view of the tracking information that will be at disposal with FTK. The main point was to perform rate reductions and efficiency evaluations. For this the JVT variable is used to suppress as much as possible the pile-up. Since it is not available online, the JVT variable of the offline jets is used to emulate an online JVT by matching the online jets to offline jets.

The impact in the rates is estimated to be reduced by 30% to 40% when JVT is considered using either topological clustering reconstructed jets and particle flow reconstructed jets for the matching. Also an additional reduction of 5% is estimated for about 10% higher pile-up. For different pile-up suppressions using the JVT variable there is no significant impact on the rate reduction as for the efficiency. Some other performance studies of Run2 data have been looked at.

Further studies can be done. The impact of JVT to the multi-jet trigger selections can be estimated by using online JVT approximations, now that the software allows for FTK tracks to be used in data and MC to directly study this effect. The online reconstruction of particle flow jets can also improve the rate savings further. The L1 inefficiency in the run2 performance estimation could be associated to the presence of close-by jets in the event. This is a hypothesis that can be evaluated with the application of isolation requirements.

Bibliography

[1] Morad Aaboud et al. "Jet reconstruction and performance using particle flow with the ATLAS Detector". In: *Eur. Phys. J.* C77.7 (2017), p. 466. DOI: 10.1140/epjc/s10052-017-5031-2. arXiv: 1703.10485 [hep-ex].

[2] G. Aad et al. "ATLAS pixel detector electronics and sensors". In: *JINST* 3 (2008), P07007. DOI: 10.1088/1748-0221/3/07/P07007.

[3] G. Aad et al. "The ATLAS Experiment at the CERN Large Hadron Collider". In: *JINST* 3 (2008), S08003. DOI: 10.1088/1748-0221/3/08/S08003.

[4] Georges Aad et al. "Jet energy measurement and its systematic uncertainty in proton-proton collisions at $\sqrt{s} = 7$ TeV with the ATLAS detector". In: *Eur. Phys. J.* C75 (2015), p. 17. DOI: 10.1140/epjc/s10052-014-3190-y. arXiv: 1406.0076 [hep-ex].

[5] Georges Aad et al. "Performance of the ATLAS muon trigger in pp collisions at $\sqrt{s} = 8$ TeV". In: *Eur. Phys. J.* C75 (2015), p. 120. DOI: 10.1140/epjc/s10052-015-3325-9. arXiv: 1408.3179 [hep-ex].

[6] Georges Aad et al. "Technical Design Report for the Phase-I Upgrade of the ATLAS TDAQ System". In: CERN-LHCC-2013-018. ATLAS-TDR-023 (2013). Final version presented to December 2013 LHCC. URL: http://cds.cern.ch/record/1602235.

[7] Georges Aad et al. "Topological cell clustering in the ATLAS calorimeters and its performance in LHC Run 1". In: *Eur. Phys. J.* (2017). DOI: 10.1140/epjc/s10052-017-5004-5. arXiv: 1603.02934 [hep-ex].

[8] A. Abdesselam et al. "The barrel modules of the ATLAS semiconductor tracker". In: *Nucl. Instrum. Meth.* A568 (2006). DOI: 10.1016/j.nima.2006.08.036.

[9] R. Achenbach et al. "The ATLAS Level-1 Calorimeter Trigger". In: ATL-DAQ-PUB-2008-001. ATL-COM-DAQ-2008-002 (2008). DOI: 10.1088/1748-0221/3/03/P03001. URL: http://cds.cern.ch/record/1080560.

[10] O. Adriani et al. "The LHCf detector at the CERN Large Hadron Collider". In: *JINST* 3 (2008), S08006. DOI: 10.1088/1748-0221/3/08/S08006.

[11] A. Airapetian et al. "ATLAS calorimeter performance Technical Design Report". In: (1996).

[12] A. Hoecker et al. "TMVA: Toolkit for Multivariate Data Analysis". In: *CERN-OPEN-2007-007* (August 2, 2018). URL: https://arxiv.org/pdf/physics/0703039.pdf.

[13] M. Aleksa et al. "Construction, assembly and tests of the ATLAS electromagnetic end-cap calorimeters". In: *JINST* 3 (2008). DOI: 10.1088/1748-0221/3/06/P06002.

[14] G. Anelli et al. "The TOTEM experiment at the CERN Large Hadron Collider". In: *JINST* 3 (2008), S08007. DOI: 10.1088/1748-0221/3/08/S08007.

[15] S. Artz et al. "Upgrade of the ATLAS Central Trigger for LHC Run-2". In: *Journal of Instrumentation* 10 (2015), pp. C02030–C02030. URL: https://doi.org/10.1088%2F1748-0221%2F10%2F02%2Fc02030.

[16] S Ask et al. "The ATLAS central level-1 trigger logic and TTC system". In: *Journal of Instrumentation* (2008), P08002–P08002. URL: https://doi.org/10.1088%2F1748-0221%2F3%2F08%2Fp08002.

[17] *ATLAS Events at 13 TeV - First 2016 Stable Beams and sketch from the slides of Anna Sfyrla (UNIGE), Summer Students Lectures, July 2018*. https://cds.cern.ch/images/ATLAS-PHO-Event-2016-003-4.

[18] "ATLAS liquid argon calorimeter: Technical design report". In: (1996).

[19] "ATLAS tile calorimeter: Technical design report". In: (1996).

[20] *Beta and Emittance, taking a closer look at LHC*. https://www.lhc-closer.es/taking_a_closer_look_at_lhc/0.beta___emittance.

[21] Matteo Cacciari and Gavin P. Salam. "Pileup subtraction using jet areas". In: *Phys. Lett.* B659 (2008), pp. 119–126. DOI: 10.1016/j.physletb.2007.09.077. arXiv: 0707.1378 [hep-ph].

[22] Matteo Cacciari, Gavin P. Salam, and Gregory Soyez. "The anti-k_t jet clustering algorithm". In: *JHEP* 04 (2008). DOI: 10.1088/1126-6708/2008/04/063. arXiv: 0802.1189 [hep-ph].

[23] Diego Casadei. "Estimating the selection efficiency". In: *2012-JINST-7-P08021* (25 July 2012). URL: https://arxiv.org/abs/0908.0130.

[24] ATLAS Collaboration. *Measurement of the photon identification efficiencies with the ATLAS detector using LHC Run 2 data collected in 2015 and 2016*. Oct. 2018.

[25] The ATLAS Collaboration. "Identification and rejection of pile-up jets at high pseudorapidity with the ATLAS detector". In: *EPJC : CERN-EP-2017-055* (8th May 2017). URL: arXiv:1705.02211v1.

[26] The ATLAS Collaboration. "Performance of pile-up mitigation techniques for jets in pp collisions at sqrt(s) = 8 TeV using the ATLAS detector". In: *Eur. Phys. J. C (2016) 76:581* (5th December 2016). URL: https://arxiv.org/pdf/1510.03823.pdf.

[27] The ATLAS Collaboration. "Performance of the ATLAS Trigger System in 2015". In: *The European Physical Journal C* (30th May 2017), pp. 1–77. URL: 10.1140/epjc/s10052-017-4852-3.

[28] The ATLAS Collaboration. "Pile-up subtraction and suppression for jets in ATLAS". In: *ATLAS NOTE: ATLAS-CONF-2013-083* (August 9, 2013). URL: http://cds.cern.ch/record/1570994/files/.

[29] The ATLAS Collaboration. "Tagging and suppression of pileup jets with the ATLAS detector". In: *ATLAS NOTE: ATLAS-CONF-2014-018* (May 14, 2014). URL: https://cds.cern.ch/record/1700870/files/ATLAS-CONF-2014-018.pdf.

[30] Caterina Doglioni. "Measurement of the inclusive jet cross section with the ATLAS detector at the Large Hadron Collider". PhD thesis. Oxford U., 2011. URL: https://ora.ox.ac.uk/objects/uuid:1d2872e7-9fc4-4dd4-90bd-0b4e96fbb327.

[31] Discussion with Dr. Alemany Reyes.

[32] Tomoya Iizawa. "The ATLAS Fast Tracker system". In: ATL-DAQ-PROC-2017-036 (2017). DOI: 10.22323/1.313.0139. URL: https://cds.cern.ch/record/2289580.

[33] Tomoya Iizawa. "The ATLAS Fast Tracker System". In: *PoS* TWEPP-17 (2017). DOI: 10.22323/1.313.0139.

[34] N. Ilic. "The ATLAS Fast Tracker and Tracking at the High-Luminosity LHC". In: *Journal of Instrumentation* 12.02 (2017), pp. C02052–C02052. DOI: 10.1088/1748-0221/12/02/c02052. URL: https://doi.org/10.1088%2F1748-0221%2F12%2F02%2Fc02052.

[35] Fabian Kohn. "Measurement of the charge asymmetry in top quark pair production in pp collision data at $\sqrt{s} = 7\,\text{TeV}$ using the ATLAS detector". PhD thesis. Gottingen U., II. Phys. Inst., 2012. arXiv: 1204.0952 [hep-ex].

[36] Maria Kuhn. "Emittance Preservation at the LHC". MA thesis. Hamburg U., 2013-03-12.

[37] W. Lampl et al. "Calorimeter clustering algorithms: Description and performance". In: (2008).

[38] *Lectures of Particules et Noyaux, of Prof. M. Pohl*. 2017.

[39] *Lectures of Physique du solide, of Prof. A. Morpurgo*. 2016.

[40] A. Miucci. "The ATLAS Insertable B-Layer project". In: *JINST* 9 (2014), p. C02018. DOI: 10.1088/1748-0221/9/02/C02018.

[41] James Pinfold et al. "Technical Design Report of the MoEDAL Experiment". In: (2009).

[42] B.G. Taylor for the RD12 Collaboration. "Timing Distribution at the LHC". In: *Presented at the 8th Workshop on Electronics for LHC Experiments* (13th September 2002), pp. 1–77. URL: https://cds.cern.ch/record/592719/files/p63.pdf.

[43] Steven Schramm. "ATLAS Jet Reconstruction, Calibration, and Tagging of Lorentz-boosted Objects". In: *EPJ Web Conf.* 182 (2018), p. 02113. DOI: 10.1051/epjconf/201818202113.

[44] M. Shochet et al. "Fast TracKer (FTK) Technical Design Report". In: (2013).

[45] *Triggering at ATLAS - slides of Prof. Anna Sfyrla (UNIGE), seminar at LAL, ORSAY, 20 January*. 2017.